EUROPEAN ORGANIZATION FOR NUCLEAR RESEARCH

CERN-PPE/91-83
8 March 1991

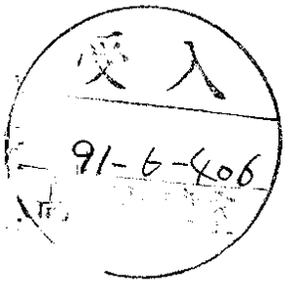

Experimental study of $\pi^-\pi^+$ system at low invariant-masses

Omicron Collaboration

G. Kernel, D. Korbar, P. Križan, M. Mikuž, F. Sever[1], A. Stanovnik, M. Starič, D. Zavrtanik[2]
J. Stefan Institute and Department of Physics, University of Ljubljana, YU-61111 Ljubljana, Yugoslavia

E.G. Michaelis[3]
CERN, CH-1211 Geneva 23, Switzerland

N.W. Tanner
Nuclear Physics laboratory, Oxford University, Oxford OX1 3RH, UK

C.W.E. van Eijk, R.W. Hollander, W. Lourens[4]
Delft University of Technology, Delft, The Netherlands

S.A. Clark,[5]
Rutherford and Appleton Laboratory, Chilton, Didcot OX11 0QX, UK

J.D. Davies, J. Lowe, S.M. Playfer[6]
Department of Physics, University of Birmingham B15 2TT, UK

J.V. Jovanovich
Department of Physics, University of Manitoba, Winnipeg, Manitoba R3T 2N2, Canada

Abstract

We report on results of an experiment to study the reaction $\pi^-p \to \pi^-\pi^+n$ in the incident pion momentum region between 295 and 450 MeV/c. A departure from phase space was observed in invariant-mass spectra and angular distributions which cannot be explained with Δ and ρ resonance production. It indicates a $I = 0, J^P = 0^+$ $\pi^-\pi^+$ final-state interaction.

(Submitted to Zeitschrift für Physik C)

[1]Present address: DPHN CEN-Saclay, F-91191 Gif-sur-Yvette, France
[2]Present address: CERN PPE, CH-1211 Geneve 23, Switzerland
[3]Deceased
[4]Present address: State University Utrecht, Utrecht, The Netherlands
[5]Present address: DEC, RDL 2B Queens House, Forbury road, Reading RG1 3JH, UK
[6]Present address: PSI, CH-5234 Villigen, Switzerland

1 Introduction

In the past three decades, $\pi p \to \pi\pi N$ reactions have been an important source of experimental data on low-energy $\pi\pi$ interaction. Most of the existing data [1] lack, however, the information about the reaction kinematics, making the results model dependent. On the other hand, the existing full-kinematics experiments [2, 3] suffer either from lack of statistics or they were performed too far above the threshold where effects of baryon resonances in the final state become important. The data show an enhancement at high $\pi^-\pi^+$ invariant-masses, which seem not to be connected to the known resonances.

In order to supplement the existing data, we have performed a measurement of four reaction channels $\pi^\pm p \to \pi^\pm\pi^+ n$ and $\pi^\pm p \to \pi^\pm\pi^0 p$. Beams of charged pions of several momenta were chosen to investigate the reactions near the threshold. The cross-sections for the $\pi^- p$ reaction channels and the $\pi^+ p \to \pi^+\pi^+ n$ channel have been published elsewhere [4, 5, 6], while the $\pi^+ p \to \pi^+\pi^0 p$ channel is still under investigation.

The existing data show in the $\pi^-\pi^+$ system an enhancement at invariant masses of a few $100 MeV/c^2$ above the threshold. It is the purpose of the present work to study in details this feature by extending the data to lower invariant masses and by analyzing the angular distributions of the $\pi^-\pi^+ n$ final state. A comparison is also made to the related processes $pp \to pp\pi^-\pi^+, \gamma\gamma \to \pi^-\pi^+$ and $J/\Psi \to \omega\pi^-\pi^+$, and to the recent measurements of the $\pi^0\pi^0$ system.

2 Data selection

The data come from the SC94 experiment performed at the CERN Synchro-cyclotron using the OMICRON spectrometer. Details of the apparatus and experimental conditions have been given in previous publications [7]. Here we give a detailed description of background processes and procedures applied for the extraction of differential cross-sections for the $\pi^- p \to \pi^-\pi^+ n$ reaction. The incoming pion momentum ranged from 295 to 450 MeV/c.

2.1 Background analysis

Since the trigger setting was such that required two charged particles in the final state, several sources contributed to the background in the incident pion momentum region between 295 and 450 MeV/c. According to the elimination criteria they can be classified into different categories.

1. Reactions with protons in the final state:
   - $\pi^- p \rightarrow \pi^- p$ elastic scattering,
   - $\pi^- p \rightarrow \pi^- p\gamma$,
   - $\pi^- p \rightarrow \pi^- \pi^0 p$.
2. The charge exchange reaction, $\pi^- p \rightarrow \pi^0 n$, and subsequent π^0 decays (from here on electromagnetic background):
   - $\pi^0 \rightarrow e^+ e^- \gamma$ (Dalitz decay),
   - $\pi^0 \rightarrow \gamma\gamma$ where one of the photons converts into an e^+e^- pair.
3. Reactions originating in target walls and outside target material.
4. Random coincidences.

The analysis of recorded data consisted of track-finding and reconstruction of a common vertex. Charged-particle tracks were reconstructed from hits in MWPC's and drift chambers by a glued-helix method [7] taking into account magnetic field inhomogeneity. A vertex was searched for by minimizing the weighted sum of squares of distances to the three tracks,

$$S = \sum_i \frac{(\vec{x}_v - \vec{x}_i)^2}{< d_i^2 >} \tag{1}$$

where $\vec{x}_v$ is the vertex point, $\vec{x}_i$ a point on track i and d_i the distance of track i to the true vertex, as obtained from Monte-Carlo studies.

In order to facilitate further analysis and background rejection, events with double beam tracks and more than two secondary particles were rejected at an early stage of the analysis. In addition, only events with one track in each secondary spectrometer arm were transmitted to further analysis.

2.1.1 Events originating in target walls

Some of the background originated in target walls where conversion of gamma rays from π^0 decays took place. It was rejected by requiring that the vertex satisfies the condition $S < 10$ [S being defined in eq. 1]. The same condition served also to remove most of the events that come from random coincidences. Its effect on $\pi^-\pi^+n$ data was monitored with a Monte-Carlo sample, as seen from Fig. 1.

A specially designed cylindrical target was made of mylar, reinforced by kevlar fibres and filled with hydrogen gas at 1.2 MPa. The large target volume (length L = 80 cm and radius R = 7.5 cm) allowed us to perform a generous fiducial volume cut at 15 cm $\leq$ L $\leq$ 70 cm and R $\leq$ 5 cm. In this way most of the background due to π^- reactions on bound nucleons and due to gamma conversion in target wall was eliminated. The proportion of remaining target wall events was determined by taking data with pressure in the target vessel reduced to about 0.1 MPa. This residual contribution was typically about a few percent.

2.1.2 Background due to random coincidences

A large proportion of the background originating from random coincidences was eliminated by requiring that both secondary particles hit the scintillator counters in a time interval shorter than 15 ns. In addition, a special type of events was observed having an opening angle of about 180^0. It was found that they belong to random coincidences between beam particles and stopped pions decay products emerging from scintillator counters and traversing the spectrometer secondary-arms. Such events were efficiently identified from a correlation between $\cos\vartheta_-$ and $\cos\vartheta_+$ (Fig. 2) where ϑ_- (ϑ_+) is the angle between the incoming particle and secondary negative (positive) particle. The number of this type of background events was the highest at low incoming pion momenta where beam intensities were large. However, it was compensated by a better separation at low beam momenta where opening angles are small. As a result, the uncertainty originating from the subtraction of random coincidences was evenly distributed over entire region of incoming pion momenta. It amounted to less than 0.5 % of the cross section.

2.1.3 Events with protons in the final state

Combined kinematical and identification criteria were used to reject background reactions with a proton in the final state. The identification was based on time-of-flight and $\Delta E/\Delta x$ measurements. The identification capability was limited since the detector was not constructed for this purpose.

The determination of the time of flight for each of the two final-state charged particles was based on a measurement of the time difference between the signal coming from the beam scintillator counter and the signal from the secondary-particle hodoscope. A correction was applied to take into account the vertex position. The obtained values and knowledge of the path lengths allowed us to calculate the particle velocities β and their energies (pc/β). A simple cut on the positive secondary-particle energy at E = 600 MeV was sufficient to eliminate the background with a slow proton in the final state. The loss of measured events was estimated from a comparison between positive and negative particle energy distributions (see Fig. 3). The remaining events with protons in the final state were eliminated by applying a cut on energy deposited in the scintillator hodoscopes as can be seen from Fig. 4. As in the case of time-of-flight cut, the effect of the selection was monitored on negative secondary-particle spectra. The cross-section error due to proton identification was estimated to be less than 1 % at all incoming pion momenta.

2.1.4 Electromagnetic background

The electromagnetic background originates from the charge exchange reaction ($\pi^- p \rightarrow \pi^0 n$) followed by the decay of π^0. It is kinematically similar to the measured reaction, particularly in the region near the $\pi^- p \rightarrow \pi^- \pi^+ n$ reaction threshold. Therefore, the elimination of events with electron-positron pairs in the final state had to be based on particle identification criteria. By using the scintillator-hodoscope pulse height (Fig. 4) we were able to separate pions from electrons for particle momenta below 100 MeV/c. The background events could already be identified by observing one particle of the e^+e^- pair, making the background elimination particularly efficient. At electron and positron momenta, both higher than 100 MeV/c, this technique could no longer be used. However, kinematic criteria could be applied which away from threshold became more efficient (see next section).

To some extent an independent test of the systematic uncertainty resulting from the above cuts can be made by introducing a kinematical variable ω. It was calculated in the center-of-mass system of the positive and negative particle, assuming that both possess the pion mass. We defined ω as an angle between the direction of the negative pion and the direction of $\pi^-\pi^+$ cms as seen from the $\pi^-\pi^+$ cms. It is typical for the $\cos\omega$ distribution to display sharp peaks at $\cos\omega = \pm 1$ for the case of electromagnetic background, contrary to what one expects for any $\pi^-\pi^+$ system near the threshold. Therefore, by comparing $\cos\omega$ distributions for the simulated electromagnetic background and the events with at least one identified electron (Fig. 5), an estimation can be made of the systematic uncertainty. The resulting error was found to decrease from 10 % of the cross section at incoming pion momentum of 295 MeV/c, to less than 1 % at momenta above 394 MeV/c.

2.1.5 Kinematical selection of $\pi^-\pi^+n$ events

As mentioned, the particle-identification criteria could not be applied to the electromagnetic background when secondary-particle momenta exceeded 100 MeV/c. On the other hand, the distribution of the scalar sum of the two momenta (Fig. 6) provided a separation from the $\pi^-\pi^+n$ events. Consequently, a criterion for separation was chosen so as to comply with the Monte-Carlo simulation. Finally, a missing-mass cut at a value of approximately 3σ of the measured distribution was applied in order to clean up the final $\pi^-\pi^+n$ sample (Fig. 7).

2.2 Monte-Carlo simulation and differential acceptance

A Monte-Carlo simulation was used to obtain the differential acceptance of the apparatus as well as to monitor the analysis and background rejection. A realistic description of the detector was included in the simulation. The detector positions were first measured with a conventional positioning apparatus, and subsequently tuned to the cosmic-ray tracks. Beam entry parameters were taken from the analysis of a beam sampling trigger. Particles were tracked through the magnetic field of the spectrometer, taking into account energy loss and multiple Coulomb scattering in materials. The decay of pions was also simulated keeping track of the resulting muons.

Reactions were generated uniformly over the beam path through the target. For the

$\pi p \to \pi\pi N$ reactions and the elastic scattering of pions a uniform phase-space distribution was used. It was provided by the GENBOD routine [8]. Dalitz-pair decays of π^0's were generated using experimental phase-shifts [9] for the charge exchange reaction $\pi^- p \to \pi^0 n$, while the subsequent $\pi^0 \to e^+e^-\gamma$ decay was calculated from the theoretical distribution of Kroll and Wada [10]. The spectrum of photons in the πp bremsstrahlung reaction followed the $1/E_\gamma$ dependence, and final-state pions and protons were taken to be distributed isotropically.

The $\pi p \to \pi\pi N$ reaction kinematics was parametrized by the standard set of four variables: squares of the pion-pion ($s_{\pi\pi}$) and pion-nucleon ($s_{\pi N}$) invariant-masses and the azimuthal (Φ) and polar (Θ) angles of the beam respective to the (x,y) production plane in the CMS, the x-axis being defined by the direction of the nucleon (see Fig. 8).

The differential acceptance of the apparatus was obtained by submitting Monte-Carlo generated events to the same analysis procedure as the measured ones. Denoting by $N_s(x_i)$ the number of analyzed simulated events with the kinematics defined by the set x_i and by $N_g(x_i)$ the corresponding number of generated events, the differential acceptance is given by

$$w(x_i) = \frac{(\frac{dN_s(x_i)}{dx_i})}{(\frac{dN_g(x_i)}{dx_i})} \times \frac{N_t}{N_s} \tag{2}$$

Here N_t is the number of reactions generated in the target and N_s the total number of tracks used. Following equation (2) the differential cross-section can be expressed as

$$\frac{d\sigma(x_i)}{dx_i} = \frac{(\frac{dN_m(x_i)}{dx_i})}{\rho_t L N_\pi w(x_i)} \tag{3}$$

where N_m is the number of measured events, N_π the number of incident pions in the beam and $\rho_t L$ the hydrogen surface density in the target.

3 Results

The apparatus phase-space coverage was checked on two-dimensional distributions. Dalitz plots ($s_{\pi\pi}$ versus $s_{\pi n}$ distributions) obtained by analyzing simulated $\pi^- p \to \pi^-\pi^+ n$ data show a good two-dimensional phase-space coverage at all incoming pion momenta as can be seen from Fig. 9. There is, however, an indication that there are regions of phase space which are not accessible by the apparatus. This follows from the two-dimensional $\cos\Theta$ versus Φ distributions showing a loss of events in the region near $\cos\Theta = 0$ and $\Phi = 0$. Due

to relatively low statistics of recorded data we could only perform acceptance corrections in two-dimensional distributions.

3.1 Final-state dynamics

In order to study final-state dynamics, we plotted acceptance corrected Dalitz plots. A clear departure from phase-space distributions was observed at almost all incoming pion momenta (Fig. 10) showing an enhancement of high $\pi^-\pi^+$ mass events. The effect has also been observed in other measurements [2, 3] on one dimensional $m_{\pi^-\pi^+}$ distributions. The corresponding spectra obtained by our experiment are shown in Fig. 11. Non-uniformity in Dalitz plots thus seems to indicate a final-state interaction which is discussed in the following sections.

3.2 $\pi\Delta$ final state

There is no known baryon resonance which can be directly produced in the $\pi^-\pi^+n$ final state in the energy range available in our experiment. Nevertheless, it is expected that the influence of the vicinity of Δ ($m = 1.232GeV/c^2, \Gamma = 0.115GeV/c^2$) resonance should be visible in the measured Dalitz plots. As it is seen from Fig. 10, we observed no significant enhancement at high π^-n masses. The four-momentum conservation

$$s + {m_n}^2 + 2{m_\pi}^2 = s_{\pi^-\pi^+} + s_{\pi^-n} + s_{\pi^+n} \tag{4}$$

connects all the possible two-particle final-states forcing the two invariant-masses to small values if the remaining one is high. Thus, the reflections between two-body final-states and the smallness of the available phase space near the reaction threshold made the analysis more complicated.

In the measured reaction, Δ^- resonance is expected to be produced more copiously than Δ^+ due to isospin reasons. This offers a possibility for detecting Δ resonance production by measuring the ratio between π^-n and π^+n invariant-mass spectra. There seems to be an indication for such an effect which is increasing with available energy (Fig. 12). Unfortunately, the statistical significance of this effect is not sufficient for any quantitative conclusions.

Angular correlations are more sensitive to final-state interactions due to interference terms. Distributions of the angle ϑ_Δ, defined as the angle between the direction of the

pion and the direction of πn cms as seen from πn cms, could reveal the presence of a Δ resonance even below its mass by showing forward-backward asymmetry. Indeed, such an asymmetry was observed (Fig. 13). Unfortunately, the region below $\cos\vartheta_\Delta = 0$ was poorly covered by the apparatus. Thus, a precise determination of the proportion of Δ production was not possible. Nevertheless, we performed a fit to the measured $\cos\vartheta_\Delta$ distributions taking into account only low angular momenta in the initial and final state (SP1, PS1 for $\pi\pi n$ phase-space background and PP1 for Δ production; for partial-wave definitions see Ref. [11]) and assuming relative angular momentum $l = 0$ in the $\pi\pi$ system. A justification for this assumption is resulting from the present measurement as will be shown in the next section. This fit yielded a value of $25 \pm 13\%$ for the Δ branching ratio at incoming pion momentum of 450 MeV/c.

3.3 $(\pi\pi)n$ final state

Although the influence of ρ production to the $\pi^-\pi^+n$ final-state dynamics is highly improbable due to the ρ mass ($m_\rho = 0.770 GeV/c^2, \Gamma_\rho = 0.153 GeV/c^2$)) lying well outside the $\pi^-\pi^+$ mass region covered by our experiment, a check on angular distributions was performed. Distributions of $\cos\omega$ (see section 2.1.4 for the definition of ω) show no structure within experimental errors at any of the incoming pion momenta (Fig. 14). Pion pairs are distributed isotropically in the $\pi^-\pi^+$ rest system, suggesting that the two pions are in a relative s-state. Moreover, we observed no forward-backward asymmetry (Fig. 15) which should be present if the influence of a spin 1 resonance were significant. Thus, we conclude that the contribution of ρ production is negligible in the energy range accessed by our experiment.

Furthermore, the mentioned enhancement in $\pi^-\pi^+$ mass spectra cannot be explained by Δ resonance production and was attributed to a spin and parity 0^+ $\pi\pi$ interaction. Since we did not observe the same effect in $\pi^-\pi^0$ and $\pi^+\pi^+$ systems [5, 6], we concluded that the isospin of the $\pi\pi$ interaction must be zero, $I_{\pi\pi} = 0$.

The shape of $\pi^-\pi^+$ mass spectra (Fig. 11) could in principle be explained by a broad $\pi^-\pi^+$ state with a mass value outside the range of $\pi\pi$ masses covered by our measurement. Although an attempt was made to fit the measured $\pi^-\pi^+$ mass spectra to such a state, it is clear that parameters of a resonance lying outside the region of our data could not

be unambiguously obtained. In addition, the shape of the measured spectra is influenced by Δ resonance production. An introduction of terms describing Δ resonance production rendered the results of the fit even less confident due to a large number of free parameters. Therefore, our conclusion is of a qualitative nature, showing that the observed departure from phase-space distributions in $\pi^-\pi^+$ invariant-mass spectra is a consequence of a strong s-wave $\pi\pi$ attraction.

Saxon et al. [3] performed a fit to their $\pi^-p \to \pi^-\pi^+n$ and $\pi^-p \to \pi^-\pi^0p$ data at incoming pion momenta of 415, 456, 505 and 552 MeV/c. They show that the observed $\pi^-\pi^+$ enhancement can be explained only by introduction of an $I = J = 0$ $\pi\pi$ interaction.

4 Discussion

There appears to exist a compelling evidence for an enhancement in the $\pi^-\pi^+$ mass spectra, as observed by different experiments, mostly covering mass regions well above the $\pi^-\pi^+$ threshold. The effect was seen in the $\pi^-p \to \pi^-\pi^+n$ reaction [2, 3] and in other processes involving $\pi^-\pi^+$ in the final state. It was extensively studied by the DM1 and DM2 experiments [12] in $\gamma\gamma \to \pi^-\pi^+$ processes, by Axial Field Spectrometer Collaboration [13] in the reaction $pp \to pp\pi^-\pi^+$ and by the MARK III and DM2 Collaborations [14, 15] in the decay $J/\Psi \to \omega\pi^-\pi^+$. Our results show that this effect persists also at masses close to the $\pi^-\pi^+$ threshold. In particular, by measuring angular distributions and invariant-mass spectra, we show that the influence of the Δ resonance is not sufficient to explain this effect.

There have been several theoretical attempts to describe the anomalous $\pi^-\pi^+$ mass spectrum at low energies. The idea of a strong $\pi\pi$ attractive interaction which gives rise to a threshold effect in the $\pi\pi$ invariant-mass distributions was put forward by Weinstein and Isgur [16] and by Barnes et al. [17]. This explanation seems to be the most favorable although some authors [18] claimed a need of a broad $\pi\pi$ resonance previously referred to as the σ or ϵ resonance with the mass and decay width values varying in a quite wide interval ($m_\sigma = 0.4 - 1.0\ GeV/c^2$ and $\Gamma_\sigma = 0.3 - 1.0\ GeV/c^2$).

The measurement of the related $\pi^0\pi^0$ system is experimentally more complicated. The early experimental results from the $\pi^-p \to \pi^0\pi^0n$ reaction [19] show no clear enhancement in the $\pi^0\pi^0$ mass spectrum in agreement with the measurement of the reaction $\gamma\gamma \to \pi^0\pi^0$

performed by the Crystal Ball Collaboration [20]. On the other hand, an evidence for a $\pi^0\pi^0$ interaction came from a measurement of the $\pi^+p \to \pi^+p\pi^0\pi^0$ reaction at 4 GeV/c^2 [21] and from preliminary results of the Brookhaven E857 experiment studying the $\pi^-p \to \pi^0\pi^0n$ reaction near threshold [22]. A clear confirmation of the low-mass $\pi^0\pi^0$ interaction was published by the DM2 Collaboration [15]. In their study of the $J/\Psi \to \omega\pi\pi$ decay they observed a large enhancement at low $\pi^0\pi^0$ masses. The obtained $\pi^0\pi^0$ and $\pi^-\pi^+$ spectra have similar shapes. In addition, the measured relative branching ratios are in good agreement with isospin prediction.

References

[1] W.A. Perkins III, J.C. Caris, R.W. Kenney, V. Perez-Mendez: Phys. Rev. **118** (1960) 1364,
Yu. Batusov, S.A. Bunyatov, V.M. Sidorov, V.A. Yarba: JETP **12** (1961) 1290,
B.C. Barish et al.: Phys. Rev. Lett. **6** (1961) 297,
L. Deahl et al.: Phys. Rev. **124** (1961) 1987,
B.C. Barish, R.J. Kurz, V. Perez-Mendez, J. Solomon: Phys. Rev. **B135** (1964) 416,
C.W. Bjork et al.: Phys. Rev. Lett. **44** (1980) 62.

[2] J. Kirz, J. Schwarz, R.D. Tripp: Phys. Rev. **130** (1963) 2481,
Yu. Batusov, S.A. Bunyatov, V.M. Sidorov, V.A. Yarba: JETP **16** (1963) 1422,
T.D. Blokhintseva et al.: JETP **17** (1963) 80,
Yu. Batusov, S.A. Bunyatov, V.M. Sidorov, V.A. Yarba: SJNP **1** (1965) 492,
T.D. Blokhintseva et al.: SJNP **1** (1965) 71,
I.M. Blair et al.: Phys. Lett. **B32** (1970) 528.

[3] D.H. Saxon, J.H. Mulvey, W. Chinowsky: Phys. Rev. **D2** (1970) 1790,
J.A. Jones, W.W.M. Allison, D.H. Saxon: Nucl. Phys. **B83** (1974) 93.

[4] G. Kernel et al.: Phys. Lett. **B216** (1989) 244.

[5] G. Kernel et al.: Phys. Lett. **B225** (1989) 198.

[6] G. Kernel et al.: Zeit. Phys. **48C** (1990) 201.

[7] G. Kernel et al.: Nucl. Instrum. Meth. **A214** (1983) 273,
D. Zavrtanik et al.: Nucl. Instrum. Meth. **A227** (1984) 237,
G. Kernel et al.: Nucl. Instrum. Meth. **A244** (1986) 367,
P. Križan, G. Kernel, F. Sever: Nucl. Instrum. Meth. **A248** (1986) 451.

[8] F. James: CERN 68-15 (1968),
F. James: Cern Program Library W515 (1975).

[9] R. Koch, E. Pietarinen: Nucl. Phys. **A336** (1980) 331.

[10] N.M. Kroll, W. Wada: Phys. Rev. **98** (1955) 1355.

[11] B. Deler, G. Valladas: Nuovo Cimento, **45** (1966) 559,
D. Zavrtanik: Ph. D. Thesis, University of Ljubljana, Ljubljana, (1987).

[12] Z. Ajaltouni et al.: Phys. Lett. **B194** (1987) 573.

[13] T. Åkesson et al.: Phys. Lett. **B133** (1983) 268.

[14] U. Mallik: J/Ψ spectroscopy from Mark III, Proc. Fourteenth SLAC Summer Institute on Particle Physics, Probing the Standard model (Stanford, CA, USA, 28 June - 8 August 1986), ed. E.C . Brennan, p. 537, SLAC PUB 4238.

[15] J.E. Augustin et al.: Nucl. Phys. **B320** (1989) 1.

[16] J. Weinstein, N. Isgur: Phys. Rev. Lett. **48** (1982) 659,
J. Weinstein, N. Isgur: Phys. Rev. **D27** (1983) 588,
J. Weinstein, N. Isgur: Phys. Rev. **D41** (1990) 2236.

[17] T. Barnes, K. Dooley, N. Isgur: Phys. Lett. **B183** (1987) 210.

[18] G.V. Efimov, M.A. Ivanov, S.G. Mashnik: JINR E2-89-780 (1989).

[19] S. Buniatov et al.: Nucl. Phys. **B42** (1972) 77.

[20] H. Marsiske et al.: Phys. Rev. **D41** (1990) 3324.

[21] G. Borreani et al.: Nucl. Phys. **B187** (1981) 42.

[22] J. Lowe, Private communication.

Figure captions

Figure 1 Vertex fit S distributions for simulated (a) and real (b) data at incoming pion momentum of 394 MeV/c.

Figure 2 $\cos\vartheta_-$ versus $\cos\vartheta_+$ correlation (a) and $\cos\vartheta_- + \cos\vartheta_+$ distribution (b) for events at the incoming pion momentum of 413 MeV/c. ϑ_- and ϑ_+ are angles between the beam particle and the negative or positive secondary track, respectively.

Figure 3 Energy spectra for positive (a) and negative (b) particles as obtained from time-of-flight measurements at the incoming pion momentum of 354 MeV/c.

Figure 4 Scintillator pulse-height spectra for positive (a) and negative (b) secondary particles at the incoming pion momentum of 354 MeV/c.

Figure 5 $\cos\omega$ distributions at incoming pion momentum of 295 MeV/c for simulated EM background data (a) and measured events with at least one identified electron with momentum below 100 MeV/c in the final state (b).

Figure 6 Distributions on sum of charged secondary particles momenta for real data (a) and simulated $\pi^- p \to \pi^-\pi^+ n$ events (b) at the incoming pion momentum of 334 MeV/c.

Figure 7 Missing-mass distribution at the incoming pion momentum of 375 MeV/c. The solid line represents a gaussian fit to the measured data.

Figure 8 Definition of coordinate frame in overall center-of-mass system (CMS).

Figure 9 $s_{\pi^- n}$ versus $s_{\pi^-\pi^+}$ distributions (Dalitz plots) for simulated data at incoming pion momenta of 295 (a), 354 (b), 413 (c) and 450 MeV/c (d). The solid line represents the calculated boundary of the phase-space not taking into account detector resolutions.

Figure 10 Acceptance corrected $s_{\pi^+ n}$ versus $s_{\pi^-\pi^+}$ distributions at incoming pion momenta of 295 (a), 315 (b), 334 (c), 354 (d), 375 (e), 394 (f), 432 (g) and 450 MeV/c (h).

Figure 11 The ratio of $\pi^-\pi^+$ invariant-mass distribution of measured events over the distribution of accepted phase-space generated events (matrix element squared) for beam momenta 315 (a), 354 (b), 394 (c), and 432 MeV/c (d).

Figure 12 The ratio between acceptance corrected π^-n and π^+n invariant-mass spectra at incoming pion momentum of 394 (a), 413 (b), 432 (c), and 450 MeV/c (d).

Figure 13 $\cos\vartheta_{\Delta^-}$ distributions at 315 (a), 334 (b), 354 (c), 375 (d), 394 (e), 413 (f), 432 (g) and 450 MeV/c (h).

Figure 14 $\cos\omega$ distributions at 295 (a), 315 (b), 334 (c), 354 (d), 375 (e), 413 (f), 432 (g) and 450 MeV/c (h).

Figure 15 $\frac{F-B}{F+B}$ asymmetry as a function of $\pi^-\pi^+$ invariant-mass. Data from all incoming pion momenta are combined on the plot. The solid line represents the result of a straight-line fit which yielded a value of 0.003 ± 0.051 for $\frac{F-B}{F+B}$.

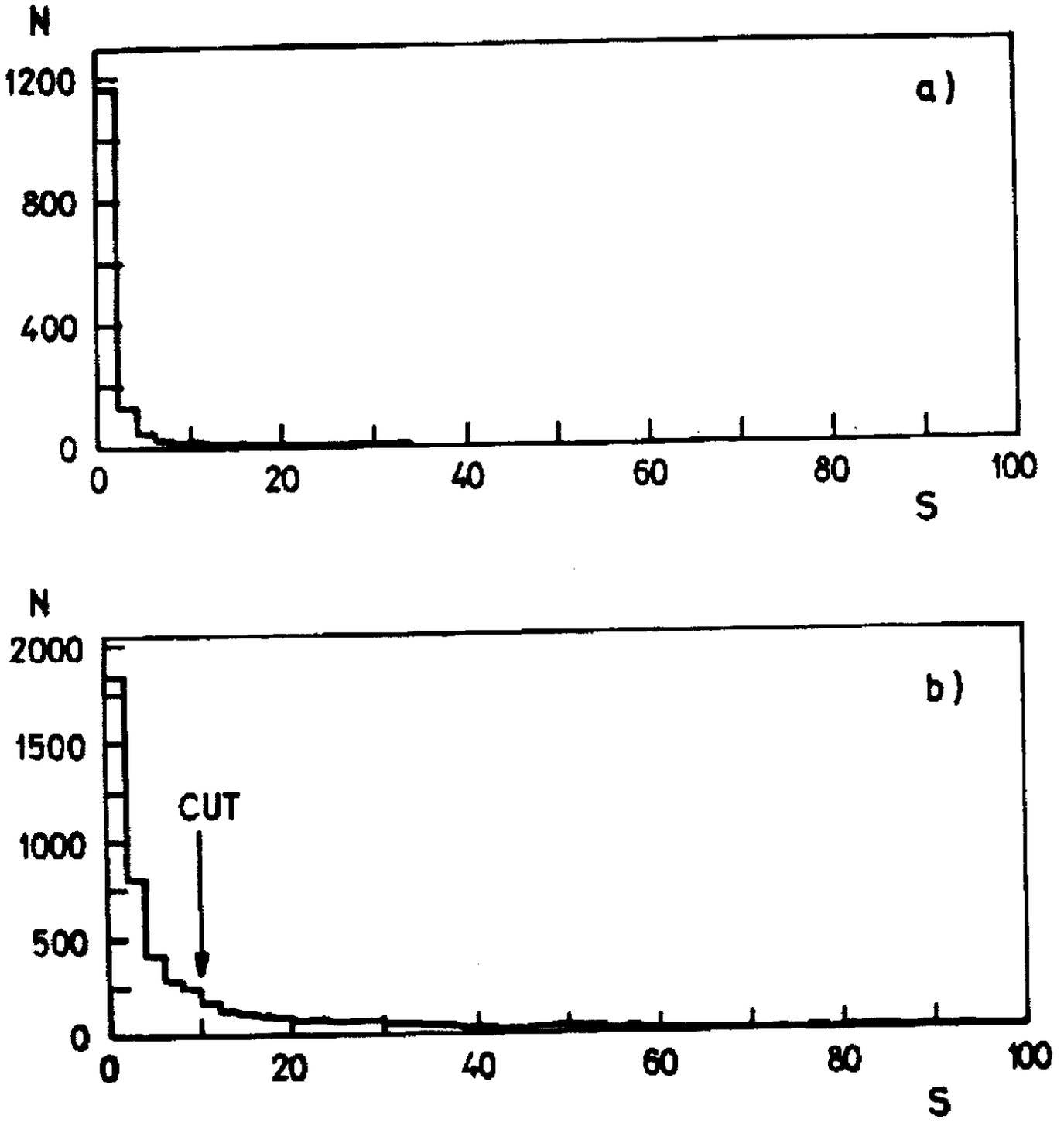
N
1200
800
400
0
a)
0
20
40
60
80
100
S
N
2000
1500
1000
500
0
CUT
b)
0
20
40
60
80
100
S

Figure 1

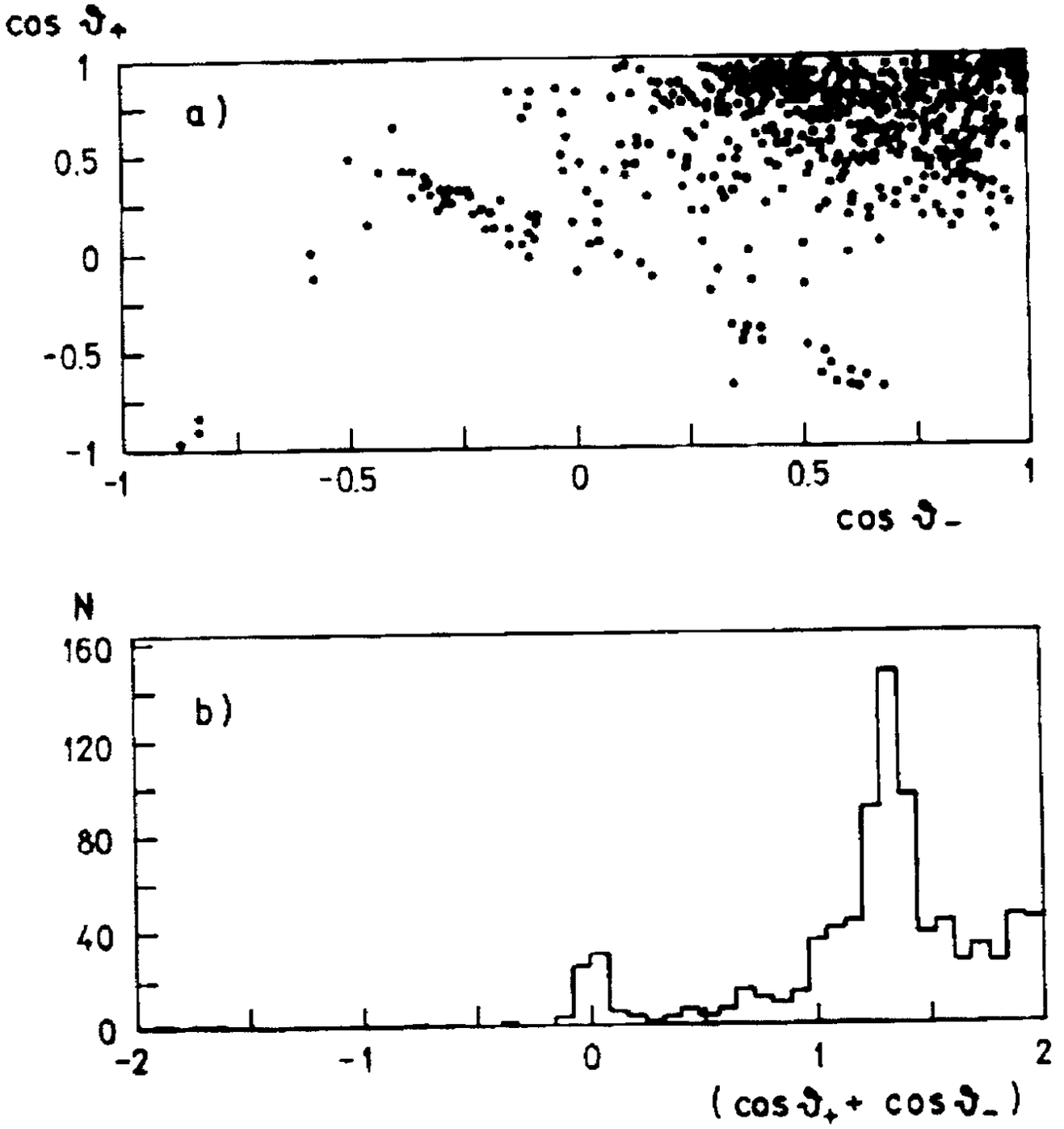

Figure 2

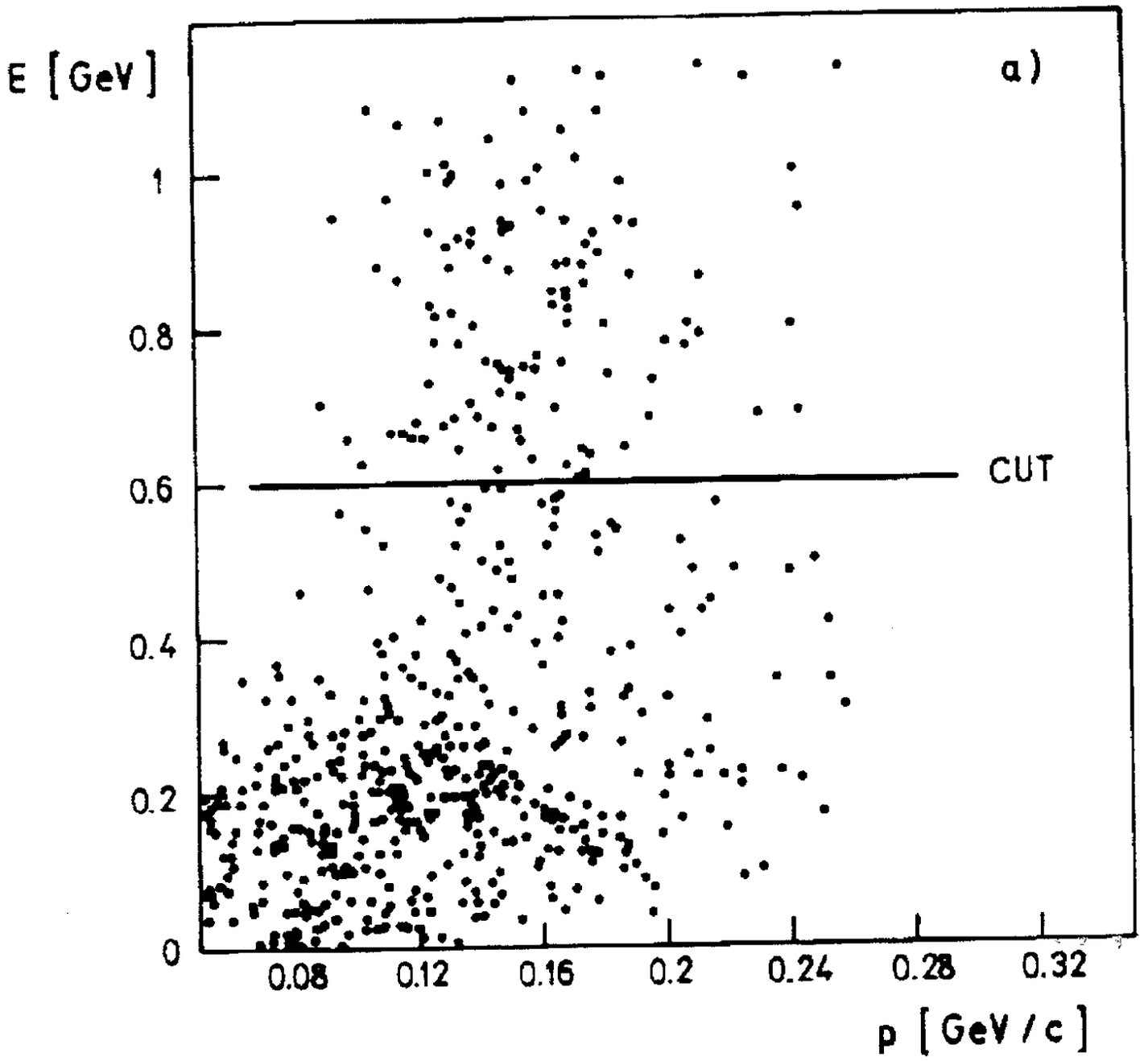

Figure 3

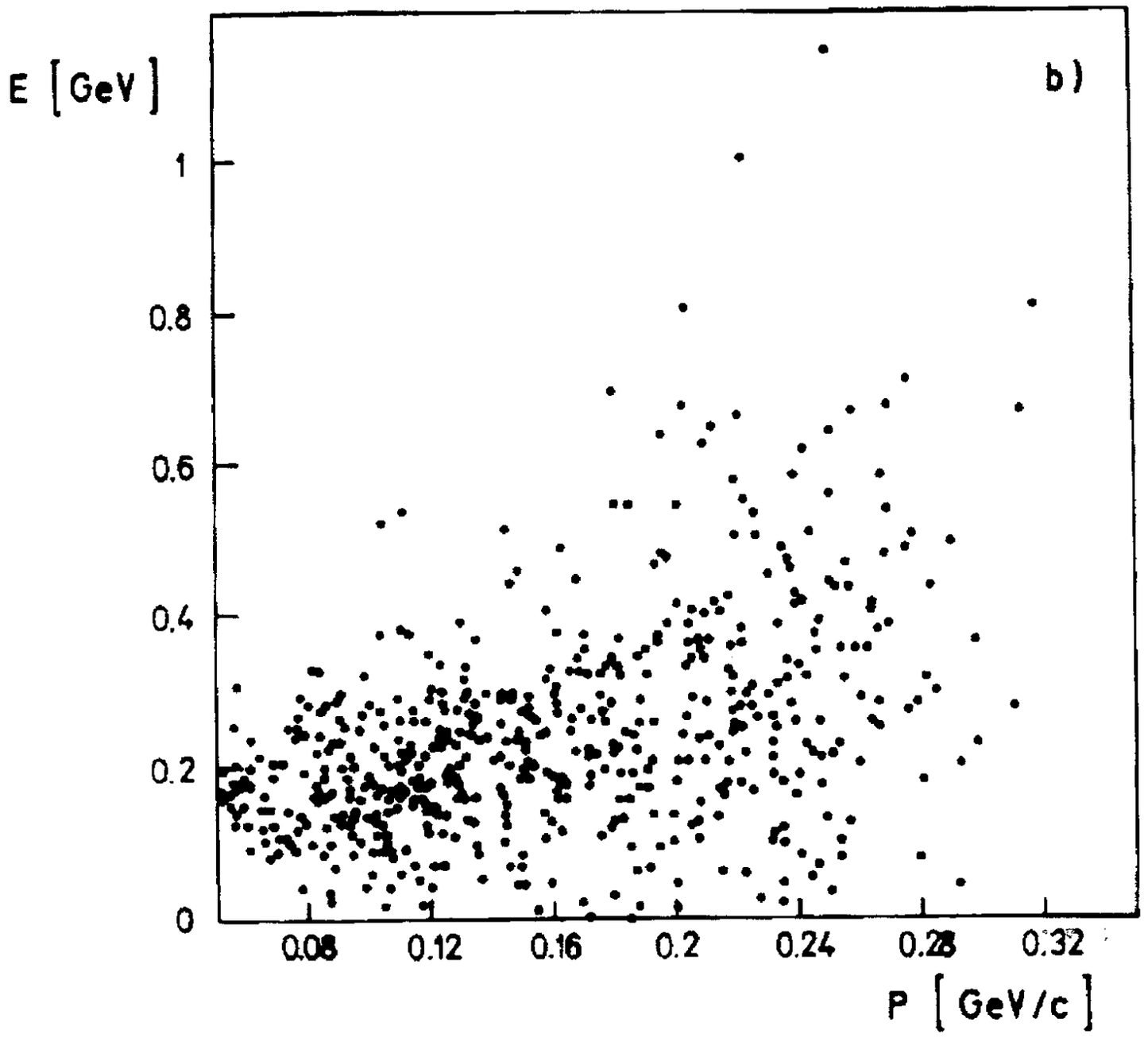

Figure 3

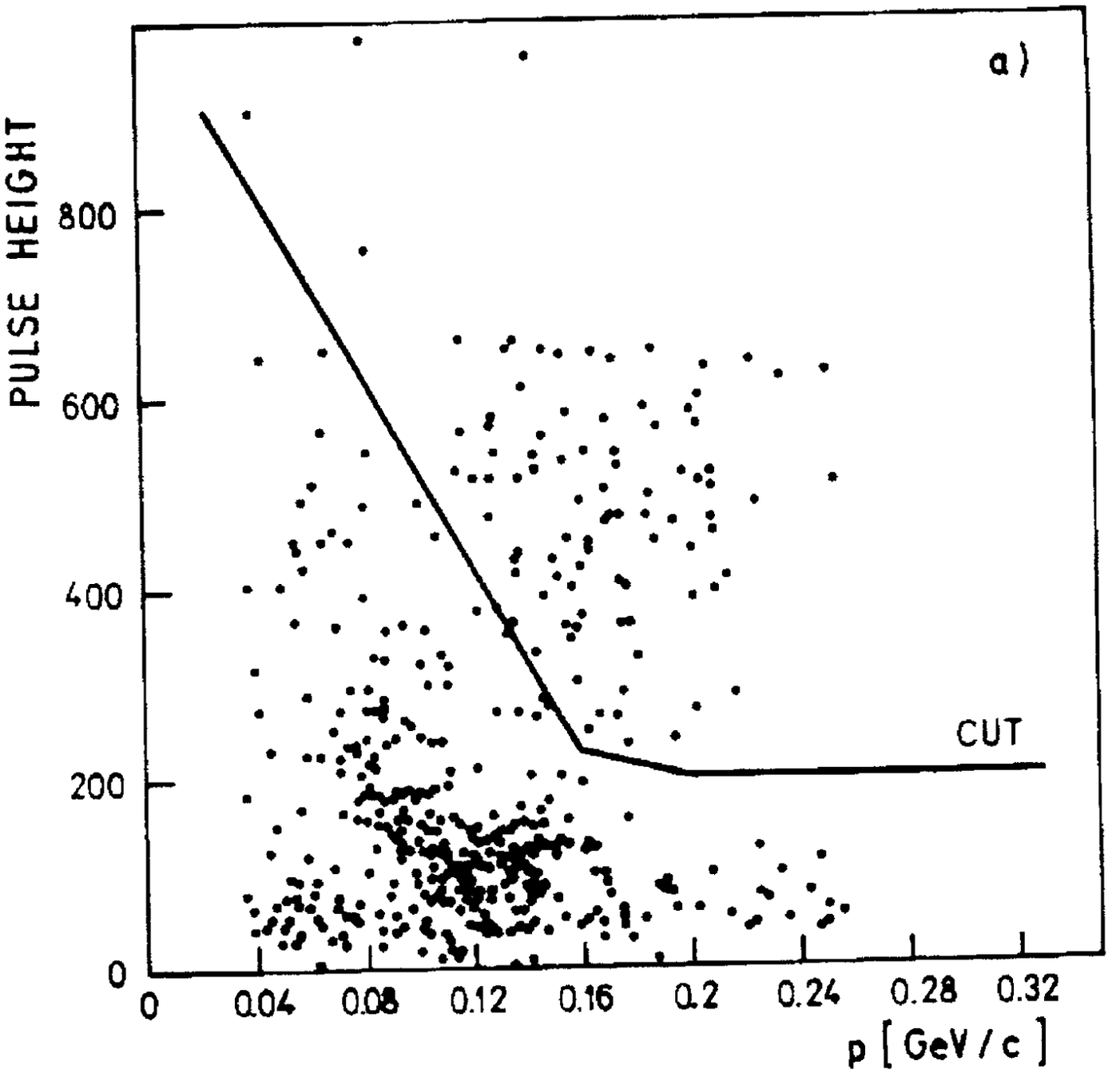
a)
PULSE HEIGHT
800
600
400
200
0
CUT
0
0.04
0.08
0.12
0.16
0.2
0.24
0.28
0.32
p [GeV / c]

Figure 4

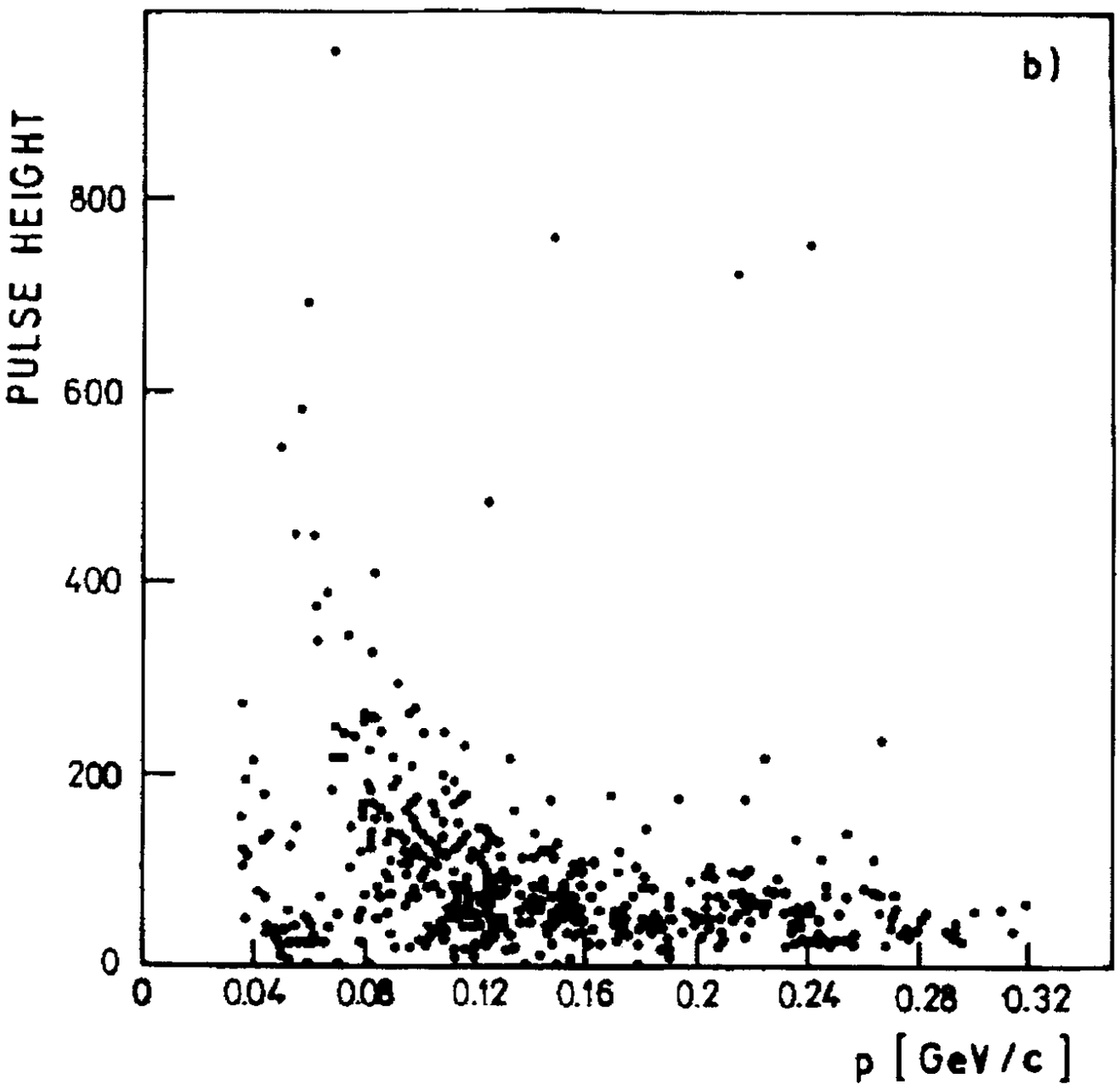
b)
PULSE HEIGHT
800
600
400
200
0
0
0.04
0.08
0.12
0.16
0.2
0.24
0.28
0.32
p [GeV/c]

Figure 4

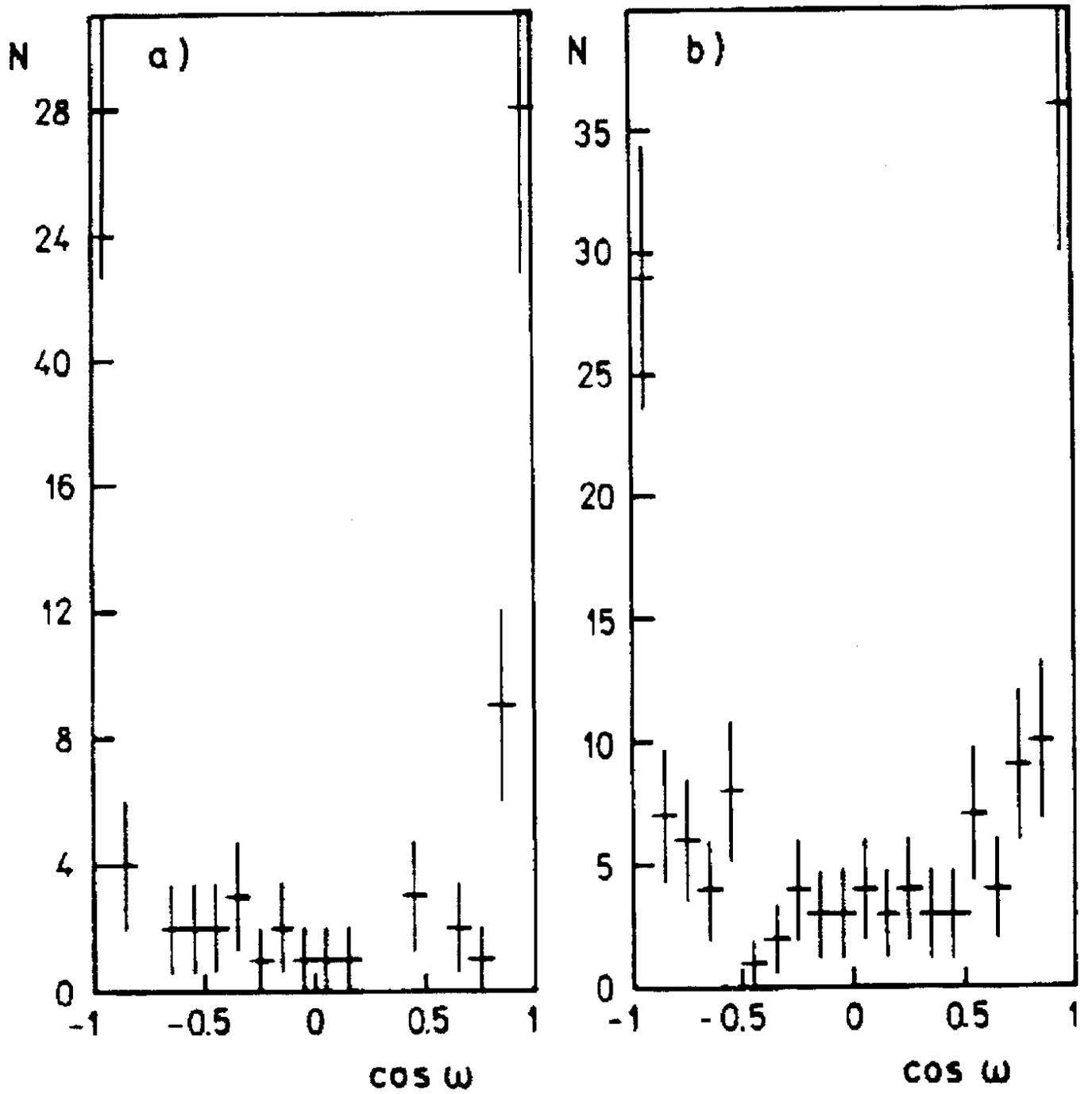
N
a)
28
24
40
16
12
8
4
0
-1
-0.5
0
0.5
1
cos ω
N
b)
35
30
25
20
15
10
5
0
-1
-0.5
0
0.5
1
cos ω

Figure 5

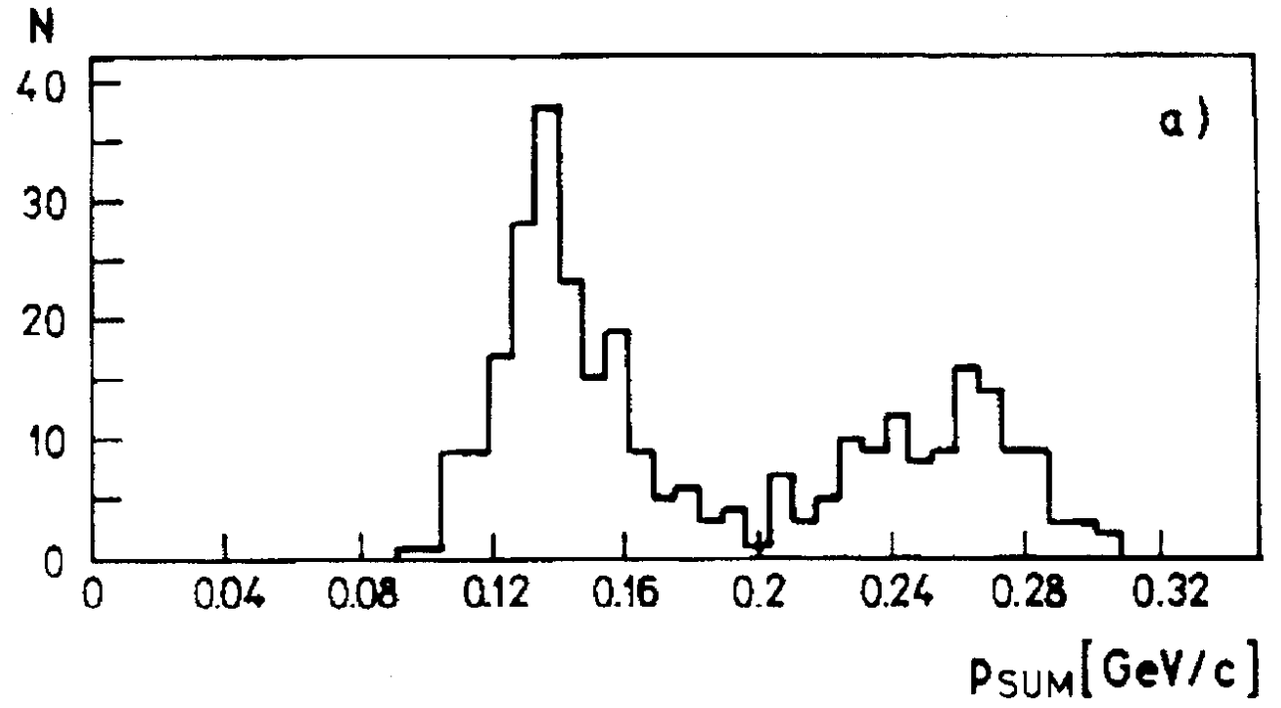
N
40
30
20
10
0
a)
0
0.04
0.08
0.12
0.16
0.2
0.24
0.28
0.32
PSUM[GeV/c]

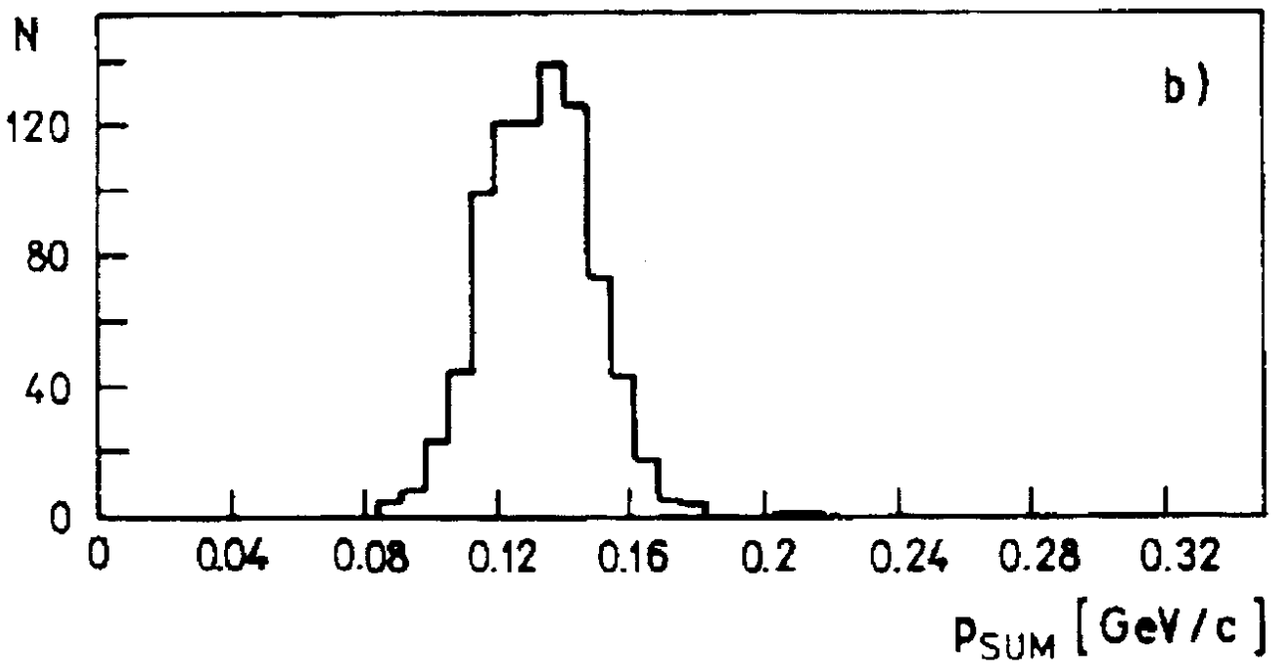
N
120
80
40
0
b)
0
0.04
0.08
0.12
0.16
0.2
0.24
0.28
0.32
PSUM [GeV/c]

Figure 6

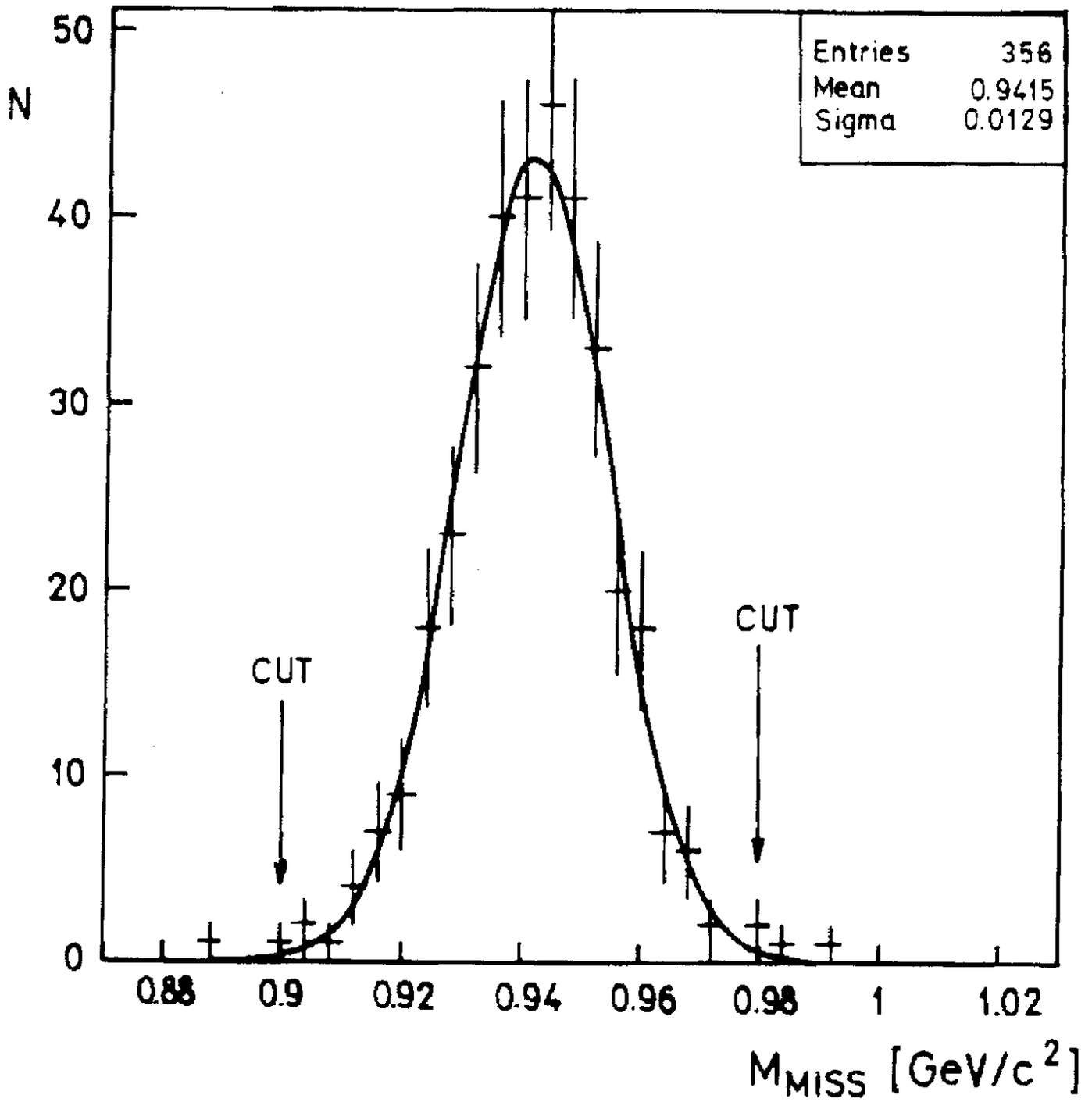
Entries 356
Mean 0.9415
Sigma 0.0129
N
50
40
30
20
10
0
CUT
CUT
0.88
0.9
0.92
0.94
0.96
0.98
1
1.02
M_{MISS} [GeV/c^2]

Figure 7

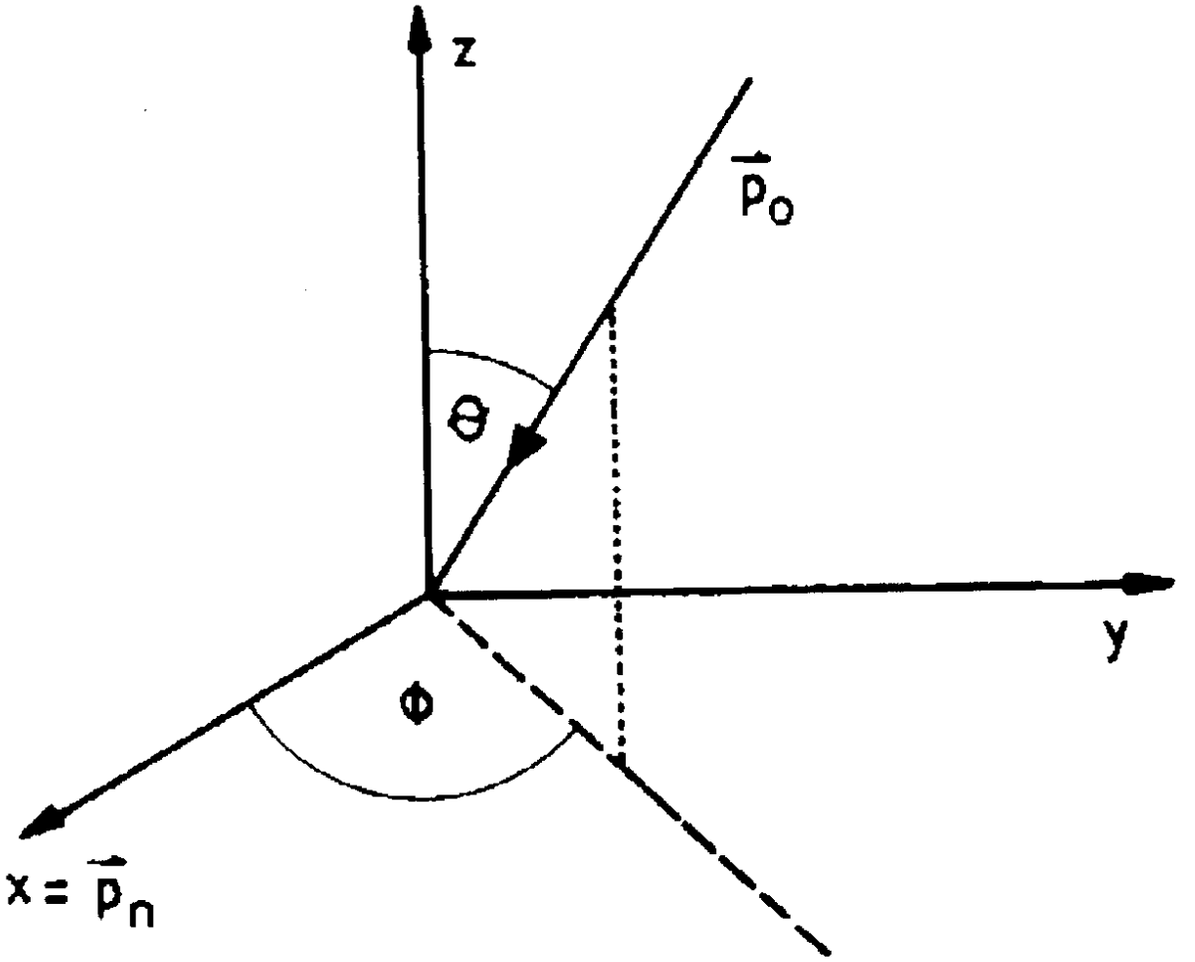

Figure 8

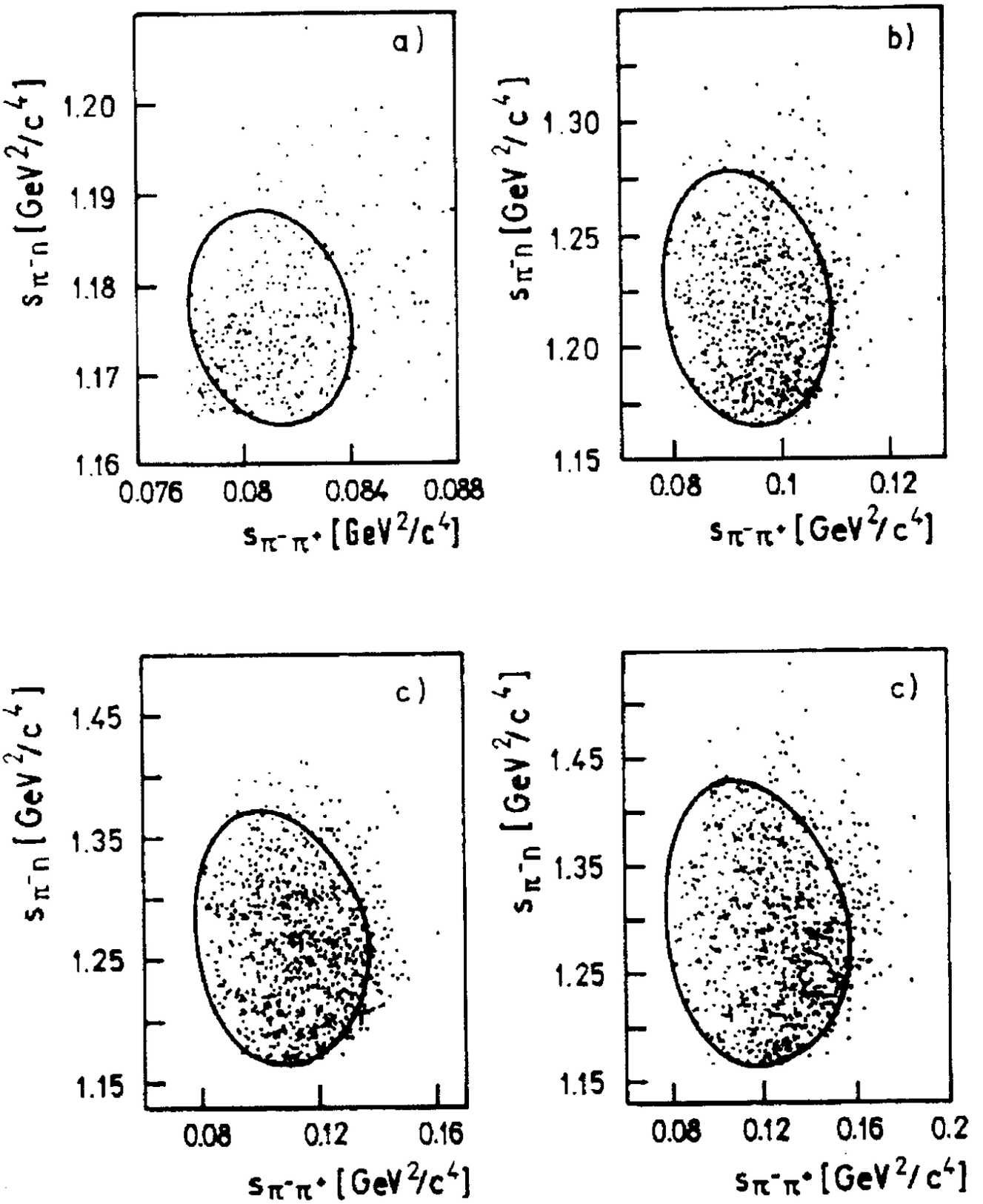
a)
b)
c)
c)
s_{π^-n} [GeV^2/c^4]
$s_{\pi^-\pi^+}$ [GeV^2/c^4]
1.20
1.19
1.18
1.17
1.16
0.076
0.08
0.084
0.088
1.30
1.25
1.20
1.15
0.08
0.1
0.12
1.45
1.35
1.25
1.15
0.08
0.12
0.16
0.2

Figure 9

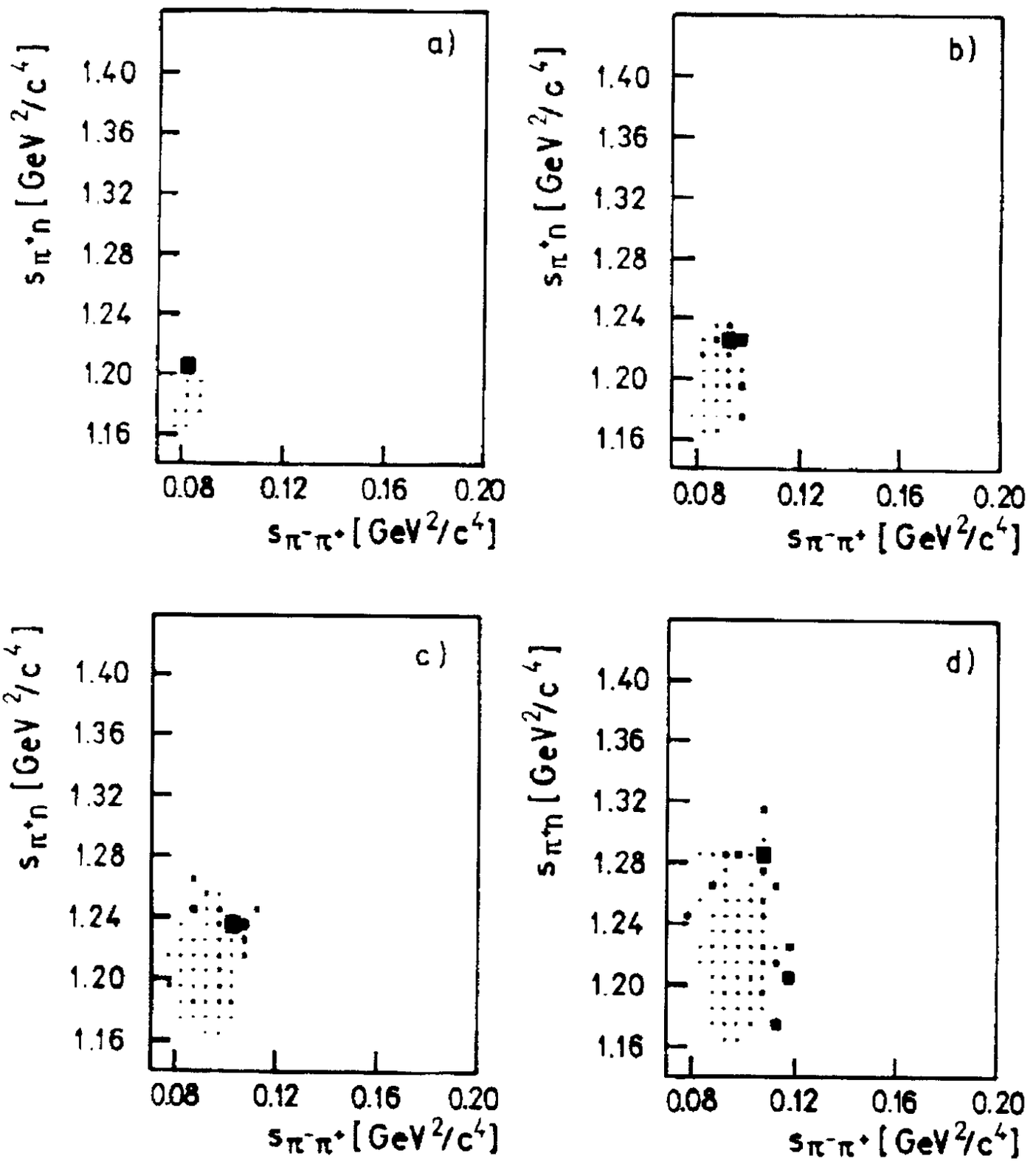
a)
b)
c)
d)
1.40
1.36
1.32
1.28
1.24
1.20
1.16
0.08
0.12
0.16
0.20
s_{π^+n} [GeV^2/c^4]
$s_{\pi^-\pi^+}$ [GeV^2/c^4]

Figure 10

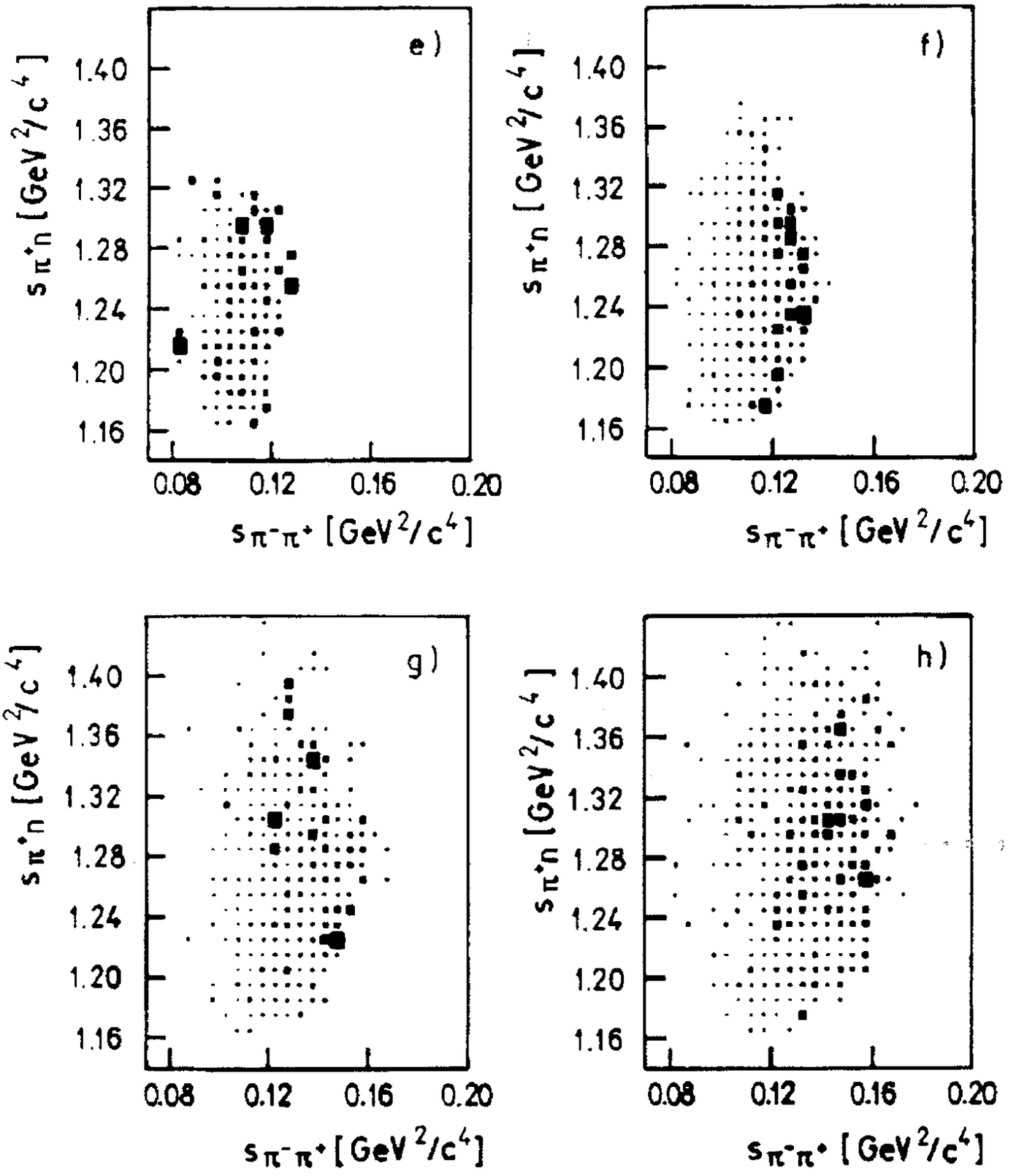
e)
f)
g)
h)
1.40
1.36
1.32
1.28
1.24
1.20
1.16
0.08
0.12
0.16
0.20
s_{π^+n} [GeV^2/c^4]
$s_{\pi^-\pi^+}$ [GeV^2/c^4]

Figure 10

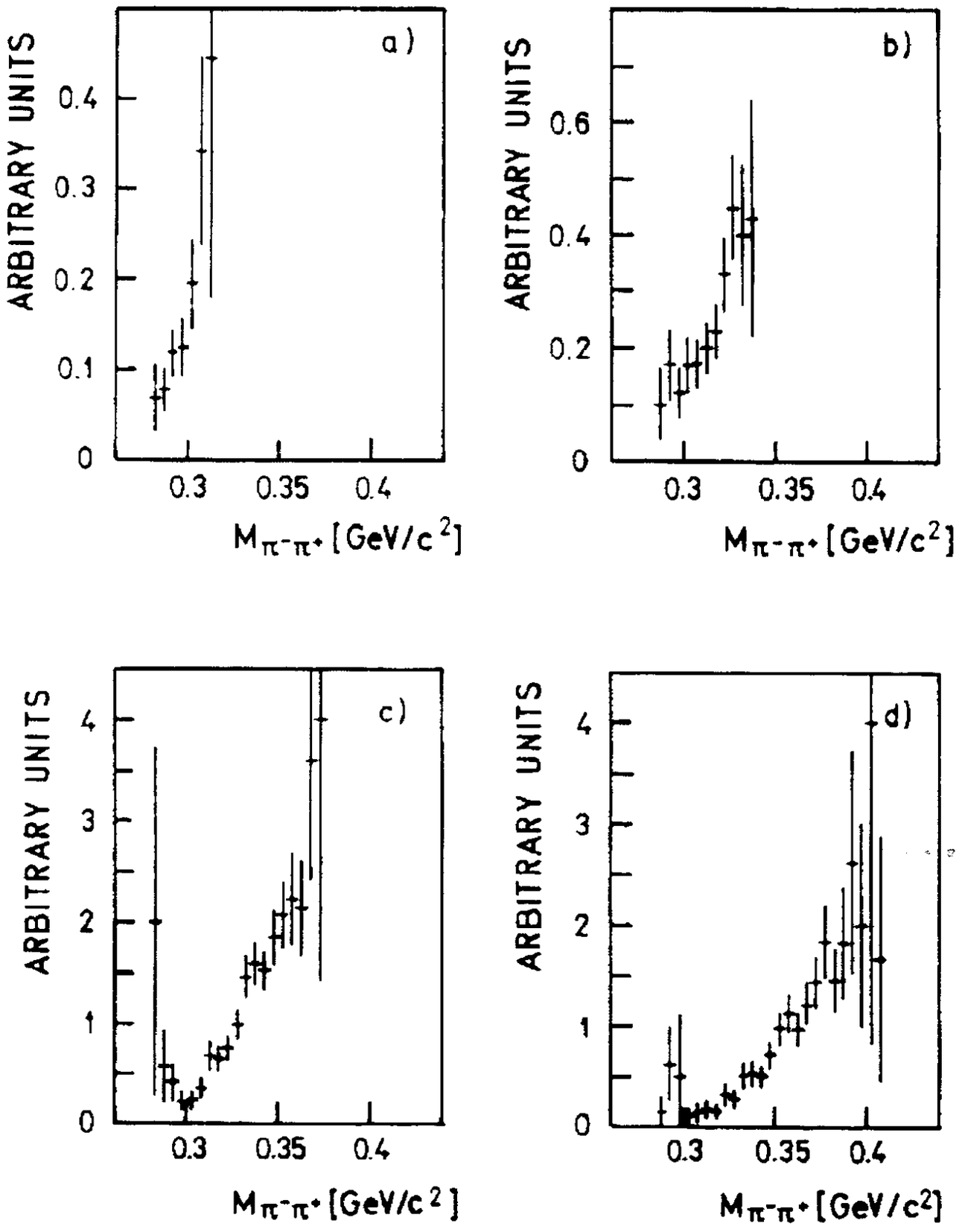

Figure 11

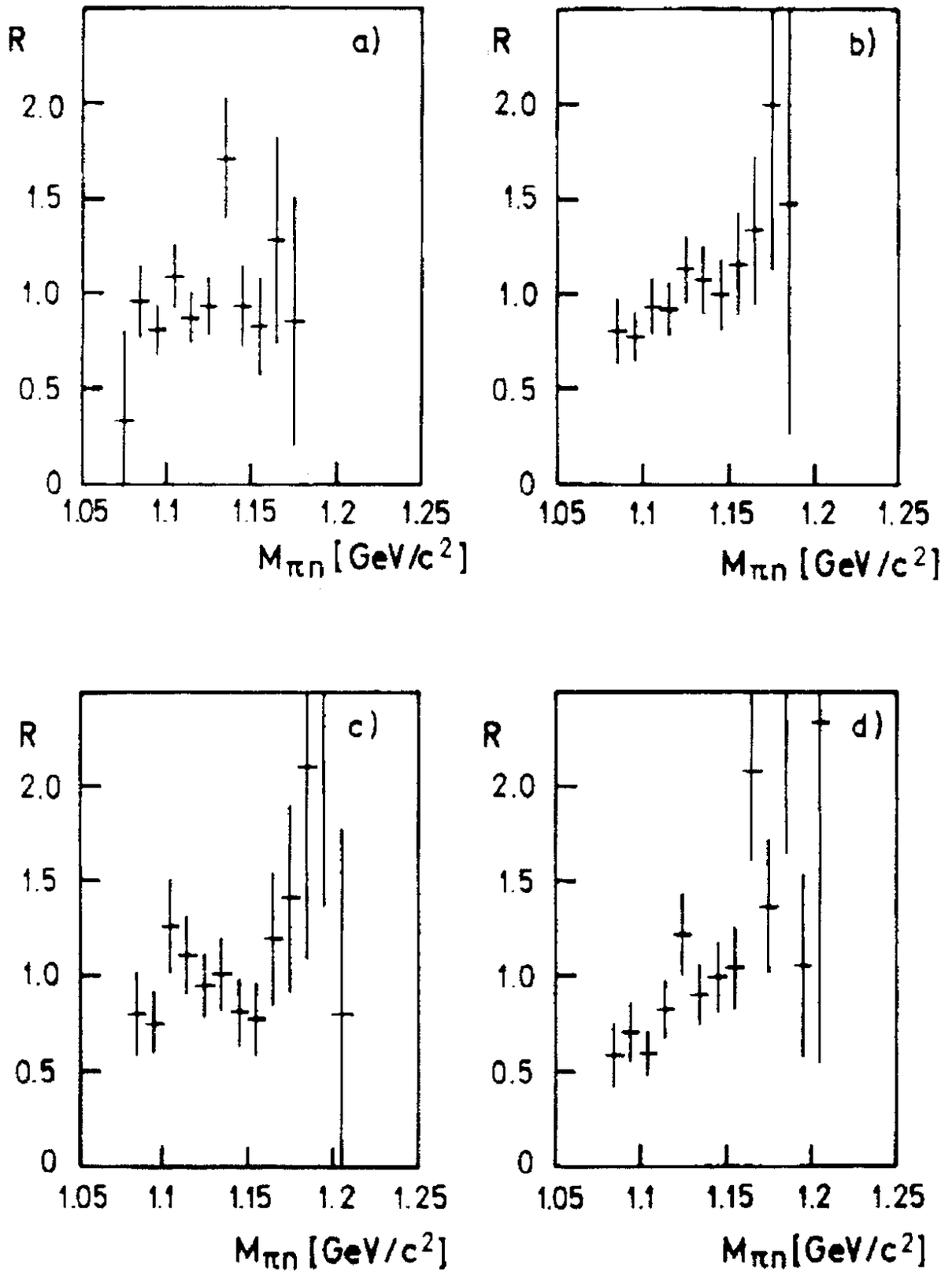
R
a)
2.0
1.5
1.0
0.5
0
1.05
1.1
1.15
1.2
1.25
$M_{\pi n}$ [GeV/c^2]
R
b)
2.0
1.5
1.0
0.5
0
1.05
1.1
1.15
1.2
1.25
$M_{\pi n}$ [GeV/c^2]
R
c)
2.0
1.5
1.0
0.5
0
1.05
1.1
1.15
1.2
1.25
$M_{\pi n}$ [GeV/c^2]
R
d)
2.0
1.5
1.0
0.5
0
1.05
1.1
1.15
1.2
1.25
$M_{\pi n}$ [GeV/c^2]

Figure 12

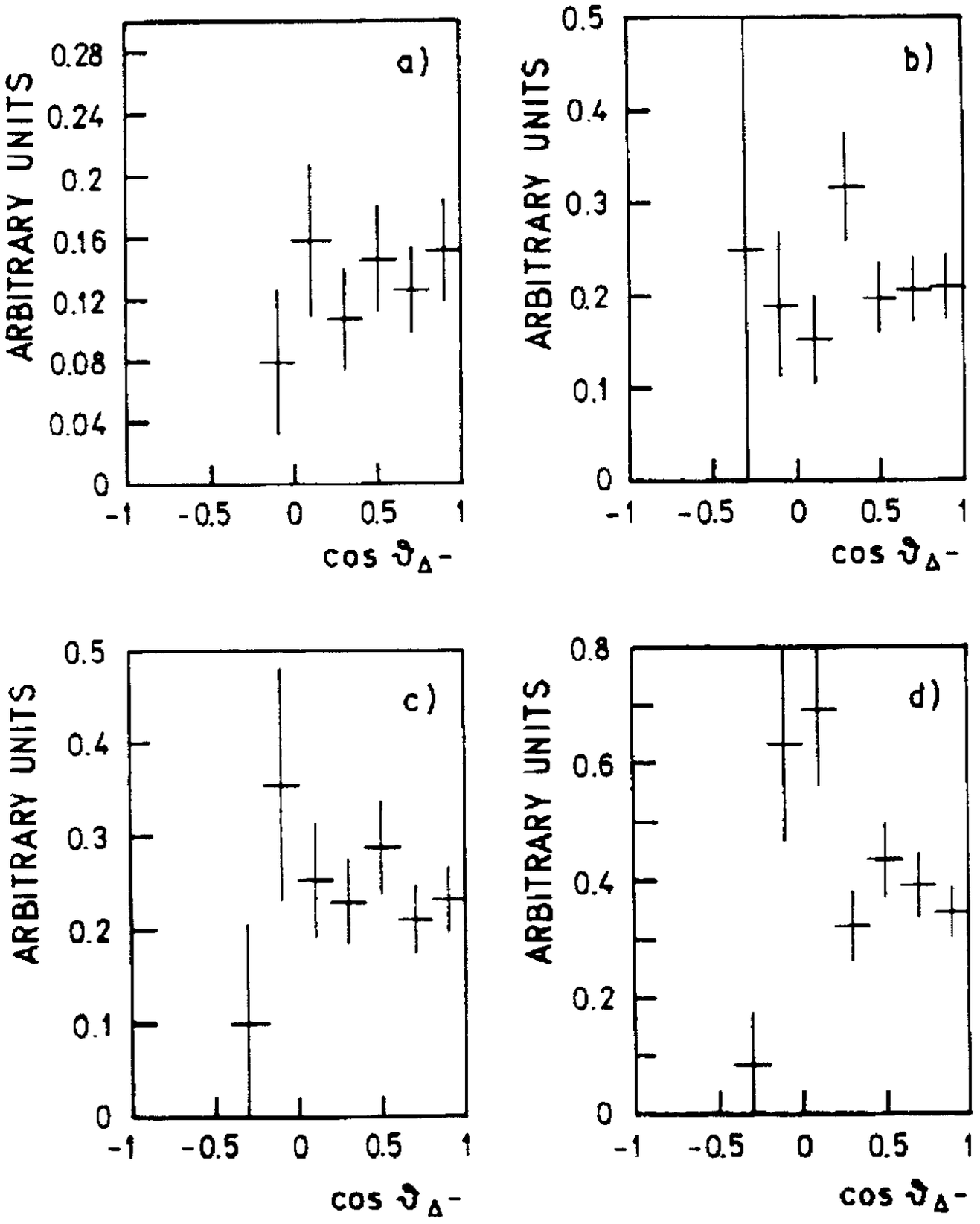
a)
b)
c)
d)
ARBITRARY UNITS
cos ϑ_{Δ^-}
0.28
0.24
0.2
0.16
0.12
0.08
0.04
0.5
0.4
0.3
0.1
0.8
0.6
-1
-0.5
0
0.5
1

Figure 13

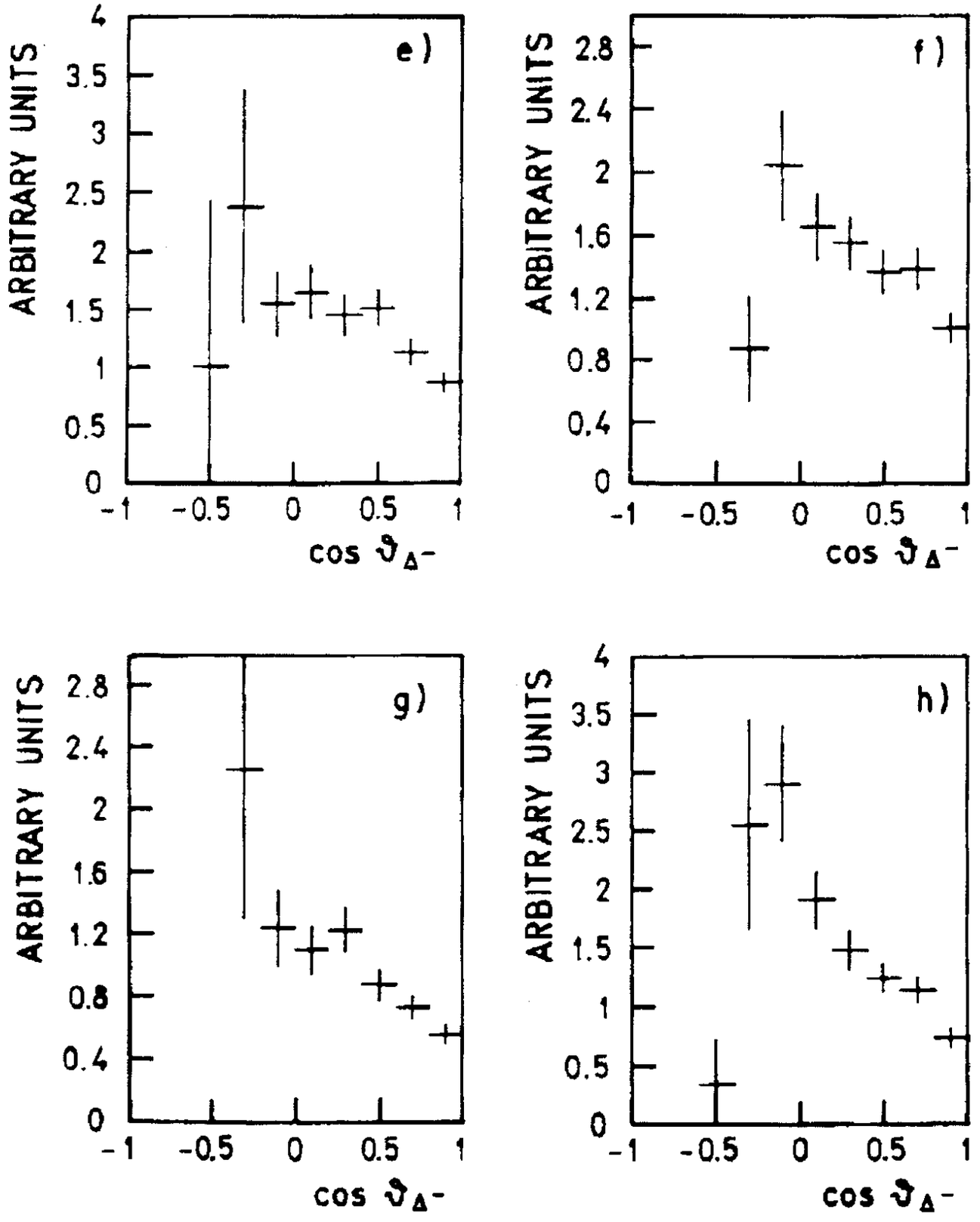

Figure 13

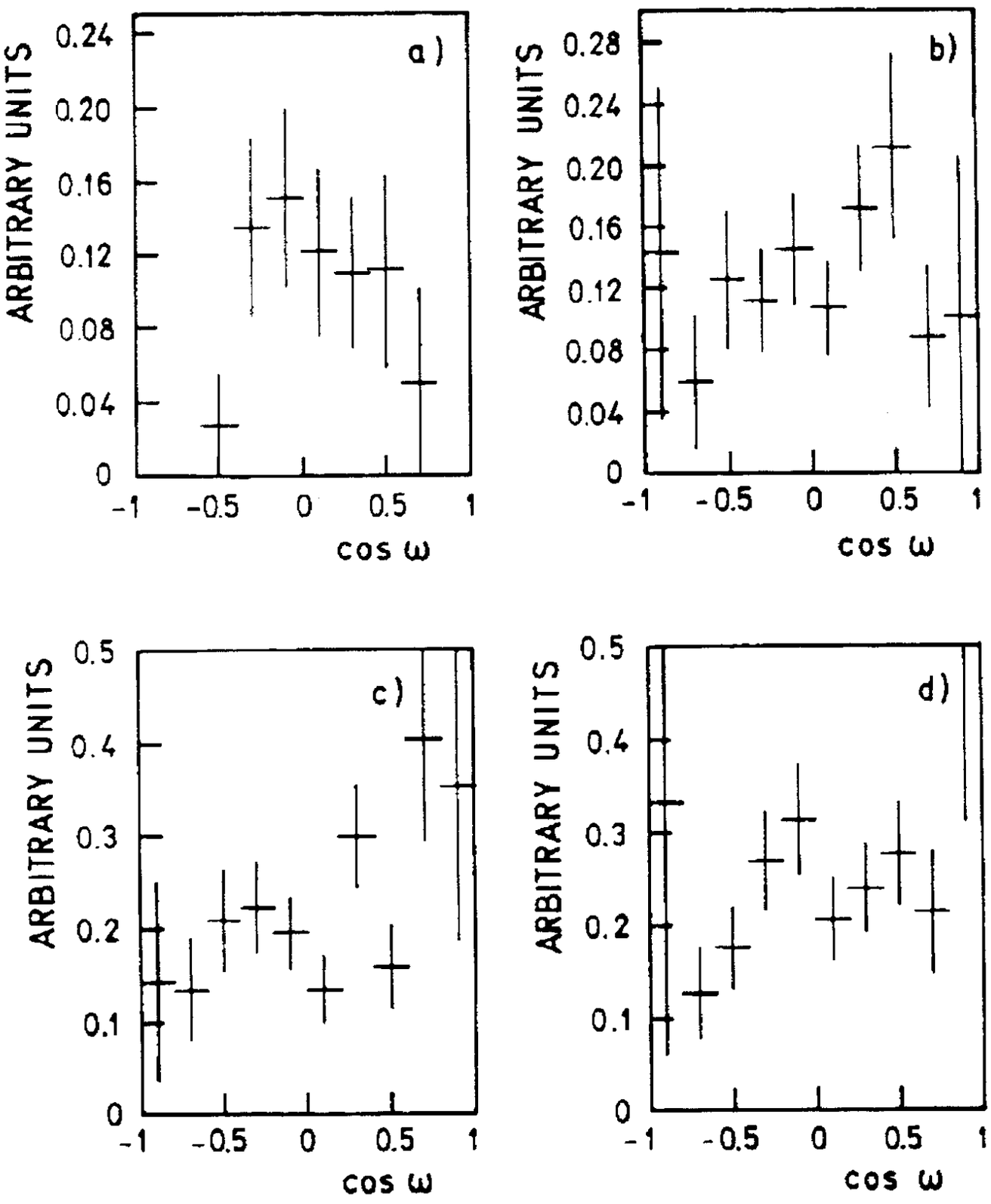
a)
b)
c)
d)
ARBITRARY UNITS
cos ω
0.24
0.20
0.16
0.12
0.08
0.04
0
0.28
0.5
0.4
0.3
0.2
0.1
-1
-0.5
0
0.5
1

Figure 14

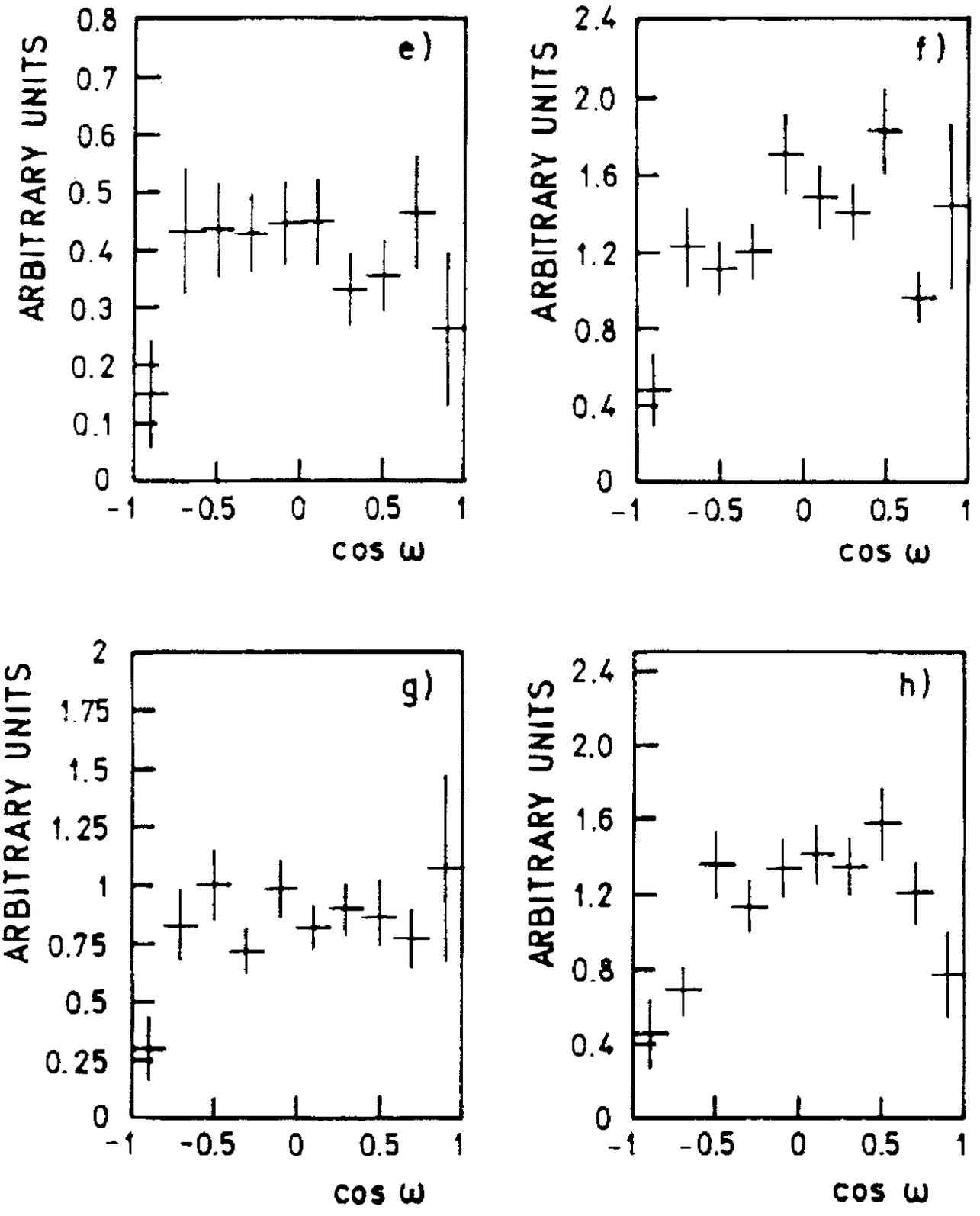
e)
f)
g)
h)
ARBITRARY UNITS
cos ω
0.8
0.7
0.6
0.5
0.4
0.3
0.2
0.1
0
2.4
2.0
1.6
1.2
0.8
0.4
2
1.75
1.5
1.25
1
0.75
0.5
0.25
-1
-0.5
0
0.5
1

Figure 14

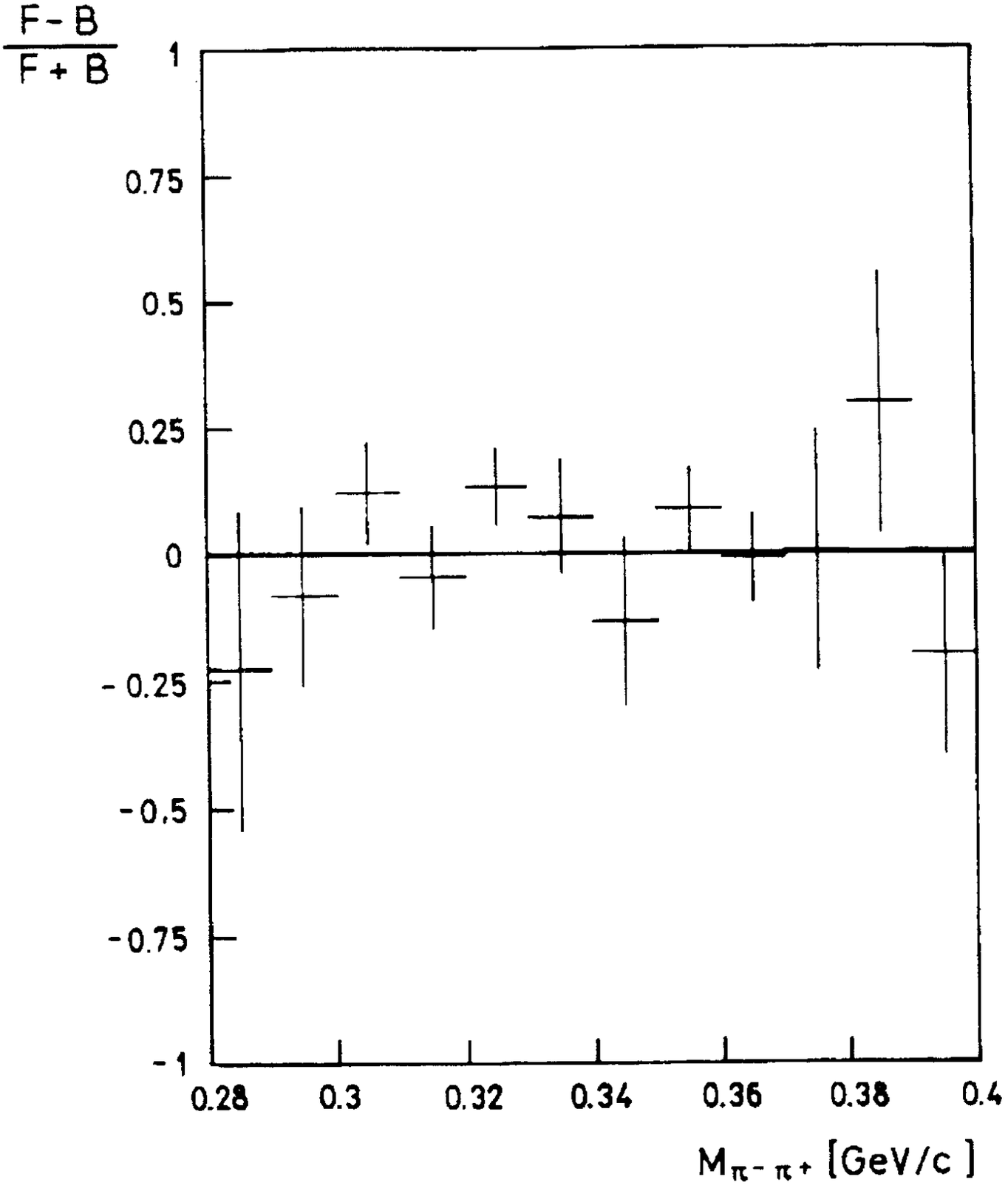

Figure 15